

AN INVESTIGATION OF THE STRATIGRAPHY AND HYDROGEOLOGY BENEATH  
THE BALL STATE UNIVERSITY GROUND – SOURCE GEOTHERMAL SYSTEM

A THESIS SUBMITTED TO THE GRADUATE SCHOOL  
IN PARTIAL FULFILLMENT OF THE REQUIREMENTS

FOR THE DEGREE  
MASTER OF SCIENCE

BY  
ANDREW SILISKI  
DR. LEE FLOREA – ADVISOR

BALL STATE UNIVERSITY  
MUNCIE, INDIANA  
DECEMBER 2014

## **ABSTRACT**

**THESIS:** An Investigation of the Stratigraphy and Hydrogeology Beneath the Ball State University Ground-Source Geothermal System

**STUDENT:** Andrew Siliski

**DEGREE:** Master of Science

**COLLEGE:** Sciences and Humanities

**DATE:** December 2014

**PAGES:** 94

Ball State University (BSU) is in the process of constructing the world's largest ground-source, district-scale geothermal system utilizing the shallow lithology and groundwater as a thermal reservoir. Data from four research wells drilled in Phase III during 2012–2013 comprise the information for this thesis. Data include well logs and cuttings as well as gamma logs collected in collaboration with the Indiana Geological Survey. Two local cores were examined at the Indiana Geological Survey to provide correlation and aid in interpretation. Complementing these data are drilling logs for the 736 boreholes drilled to accommodate the heat exchange loops. These data were examined to construct a detailed stratigraphic log and a map of subsurface geology for the Phase 2 field. Core samples were taken at lithostratigraphic markers to measure porosity and thermal conductivity, the two key parameters in geothermal reservoir characterization. These samples were sent to Core Labs in Houston, TX to measure permeability. Although local stratigraphy is generally known, a detailed stratigraphic architecture combined with measured thermal and hydrogeological properties will aid the understanding of the true nature of the subsurface capacity to store and transport thermal energy.

## **Acknowledgments**

Thank you to my advisor, Dr. Lee Florea, for constant support in research and writing without whom this research would not have been possible. Thank you to the rest of my committee, Dr. Carolyn Dowling and Dr. Richard Fluegeman, who aided considerably in analysis and interpretation throughout the research process. This thesis was funded by the Geological Society of America, BSU Aspire, and the BSU geology department.

## Table of Contents

Title Page.....	1
Abstract.....	2
Acknowledgements.....	3
Table of Contents.....	4
Introduction.....	7
<i>1.1. Review of District-Scale GCHPs</i>	
<i>1.2. Geothermal systems and modeling in GCHPs</i>	
<i>1.3. Aquifer Permeability and Thermal Conductivity in GCHPs</i>	
Physical Setting of the Ball State University GCHP.....	12
<i>2.1. Geology of East Central Indiana</i>	
<i>2.2. Hydrology of East Central Indiana</i>	
<i>2.3. Climate of East Central Indiana</i>	
Methodology.....	15
<i>3.1. Electrical Resistivity Tomography</i>	
<i>3.2. Monitoring Well Logs and Cuttings</i>	
<i>3.3. Borehole Gamma, Resistivity, and Spontaneous Potential</i>	
<i>3.4. Bedrock Cores</i>	



### *3.5. Matrix Permeability and Porosity*

Results.....	20
<i>4.1. Pre-glacial bedrock surface and glacial stratigraphy</i>	
<i>4.2. Bedrock stratigraphy and structure</i>	
<i>4.3. Thermal stratigraphy</i>	
Discussion.....	25
<i>5.1 Surficial and Glacial Geology</i>	
<i>5.2. Ordovician–Silurian Stratigraphy of East-Central Indiana</i>	
<i>5.3. Thermal Conductivity Measurements vs. Standard Thermal Tests</i>	
<i>5.4. Hydraulic Conductivity and Porosity vs. Existing Hydrogeology Data</i>	
<i>5.5. Predicting Groundwater Temperature Changes and Comparing to Existing         Data</i>	
<i>5.6. Thermofacies</i>	
Conclusions.....	37
References.....	39
Figures.....	44

*Figure 1: Map of the Ball State University Geothermal System*

*Figure 2: Map of the Study Area*

*Figure 3: Composite Stratigraphy Column of Study Wells 1-4*

*Figure 4: N-S Transect of Study Area*

*Figure 5: W-E Transect of Study Area*

*Figure 6: Depth to Bedrock Map of Study Area*

*Figure 7: Porosity vs. Depth of the Irving Bros. Core*

*Figure 8: Mean Thermal Conductivity Dry vs. Depth of the Irving Bros. Core*

*Fig 9: Mean Thermal Conductivity Saturated vs. Depth of the Irving Bros. Core*

*Figure 10: Mean vs. Saturated Thermal Conductivity of the Irving Bros. Core*

*Figure 11: Bulk Porosity vs. Mean Saturated Thermal Conductivity of the Irving Bros. Core*

Tables.....55

*Table 1: Summary*

*Table 2: Mean Dry Thermal Conductivity of Irving Bros. Core*

*Table 3: Mean Saturated Thermal Conductivity of Irving Bros. Core*

*Table 4: Bedrock Dip and Dip Direction of Research Area*

*Table 5: Matrix Permeability of Irving Bros. Core*

*Table 6: Porosity of Irving Bros. Core*

Appendix.....61

*Appendix 1: Geophysical Well Logs*

*Appendix 2: Core Logs*

*Appendix 3: ERT Inversion Models from Mundell et al. (2012)*

## 1. Introduction

Ground-coupled heat pump systems (GCHPs) are an efficient, renewable energy source for heating and cooling (Curtis et al., 2005; Freedman et al., 2012; Sanner et al., 2003). They are becoming more widespread in the US and Europe including Germany, Switzerland, Sweden, Norway, the United Kingdom. In the U.S., GCHP systems have become more common at universities, for example Hampton University (Hampton, VA), Lipscomb University (Nashville, TN), and Minot State University (Minot, ND) (*Geothermal Systems*, n.d.). Particularly interesting examples have been installed at Stockton College (Stockton, NJ) (Taylor et al., 1998), West Chester University (Helmke et al., 2013), and The Ohio State University (Columbus, OH) (Bair and Torres, 2011).

### *1.1. Review of District-Scale GCHPs*

As of 2005, over 600,000 GCHP systems were installed in the U.S. continuing to reduce operating costs from fuel consumption and pollution from fossil fuels (Curtis et al., 2005). After their GCHP system was installed, Galt House in Louisville now consumes only 53% of the energy of adjacent, similar-sized facilities (Lund et al., 2004). The combined geothermal system at Ball State University eliminates the annual consumption of 36,000 tons of bituminous coal and should reduce total CO<sub>2</sub> emissions by 50%. Reporting on the EPA website [ghgdata.epa.gov](http://ghgdata.epa.gov) has shown a stark reduction in BSU emissions. Annual cost savings from cost of use is estimated at 2 million/yr.

Several configurations of ambient temperature systems are possible (Banks, 2008; Freedman et al., 2012) including both ‘open’ and ‘closed’ loop systems as well as systems with horizontal and vertical borehole heat exchangers (BHEs). Closed loop GCHPs are the industry

standard with vertical borehole systems outnumbering horizontal systems (Armitage et al., 1980). GCHPs rely on the ground as an energy ‘reservoir’. In the summer, heat is taken from facilities through air-conditioning and ‘deposited’ into the ground. In the winter, heat is ‘withdrawn’ and used to keep the facility warm. This energy ‘banking’ is predicted to result in a thermal cycling of the surrounding ground temperature—increasing during the summer and decreasing during the winter.

The scale of GCHPs have increased during the past decade utilizing centralized energy-transfer stations and a distribution network of heated and chilled water. As a result of increased size, maintaining thermal balance in the subsurface between periods of heating and cooling has become a significant challenge. Another significant problem in maintaining thermal balance is that geothermal systems are not always built into areas where total annual heating equals total annual cooling. Systems which are cooling-dominated will increase the ground temperature while those that are heating-dominated will decrease the ground temperature (Pertzborn et al. 2011). This annual difference will accumulate over time decreasing system efficiency requiring additional sources of heating or chilling that may negate the positive impacts of these green energy initiatives. In addition to the geothermal system, BSU has installed natural gas burners to offset any inability of the geothermal heating/cooling system. Cooling towers are also being built to correct the observed rise in temperature changes in an anticipated cooling dominant climate.

Subsurface temperatures in small-scale geothermal systems are more easily maintained. For example, long-term measurements of a residential GCHP in Elgg, Switzerland have shown only a 1–2 °C shift of ground temperatures in over 15+ years of operation, and most of that shift occurred during the first year (Rybach and Eugster, 2002). However, for district-scale GCHPs, less empirical information is available. In the Netherlands, the award-winning Schoenmakershoek

residential development near Etten-Leur proposed 1,400 residential units connected to ~2,500 BHEs in 2006 (Witte et al., 2006). Computer simulations for the Etten-Leur project suggest that significant cooling of groundwater could occur during long-term heating (Witte et al., 2006). The Stockton College GCHP system in New Jersey, one of the more published examples and activated in 1994, is comprised of 400 BHEs that are each 130 m deep and arranged in a 4.6 m grid (Taylor et al., 1998). Monitoring data from the Stockton GCHP suggest a significant heating of groundwater with a plume of ‘heated’ groundwater with temperatures between 7-11 °C above baseline values within a year of activation (Epstein et al., 1996; Epstein, 1998; Epstein and Sowers, 2006). Research by Dunn (2013) show that groundwater temperatures at BSU have increased significantly since operation and are currently at 31 °C.

### *1.2. Geothermal systems and modeling in GCHPs*

Physical characterization of the geology and hydrogeology underlying potential GCHP projects is rarely extensive. For example, as pointed out by Diao (2004), nearly all design tools for GCHP systems are based on lithological heat conduction only and ignore hydrogeological parameters. Currently, industry standard to compute the number, depth, and style of BHEs to be used in GCHPs is the borehole thermal response test (TRT). In these tests, input and output temperature is monitored over time within fluid pumped through a single BHE. From the temperature data, average values of thermal conductivity are computed assuming homogenous lithology and disregarding subsurface water flow. In general, this method may be overly simplistic from the standpoint of system design and COP and neglects potential migration of thermal plumes, such as has been observed in the Stockton GCHP, or variations in thermal conductivity in layered sedimentary aquifers.

With TRTs, heat is assumed to be stored in or removed from a homogenous and isotropic media within a uniform cylinder around the BHE. The differences in thermal and hydraulic properties of layers of soil and bedrock may cause the stored heat to extend more into strata with greater permeability and thermal conductivity. Geothermal systems are further complicated by groundwater flow will skewing stored heat into a plume disrupting the thermal balance by making stored heat unavailable during times of heat extraction.

### *1.3. Aquifer Permeability and Thermal Conductivity in GCHPs*

Permeability and thermal conductivity are the two key parameters in characterizing geothermal capacity. The library of literature addressing thermal conductivity (laboratory setting) is extensive covering all types of lithology and minerals and are best summarized by Robertson (1987). In relation to geothermal design, hydraulic conductivity is studied primarily for heat plume migration and severity (Dunn, 2013; Freedman et al., 2012). The number of publications where both are measured is, however, very low (Sass and Gotz, 2012). As a result, there is little research to base a complete comparison off of. In order to address this problem, Sass and Gotz (2012) introduced the term ‘thermofacies’ to characterize the combination of thermal conductivity and hydraulic conductivity for geothermal characterization. Sass and Gotz (2012) consider both primary and secondary rock permeability, local tectonics and double porosity, karst, and thermal conductivity and other thermophysical rock parameters.

Current research by Ellett (2014) from the Indiana Geological Survey supports targeting specific zones with favorable thermofacies for shallow geothermal heating/cooling systems. Their research, including locations at BSU, show that thermal conductivity of shallow geothermal reservoirs vary seasonally in glacial outwash sediments while clay dominated

morraines (at BSU) range less than 10% of the annual mean (Ellett and Naylor, in review).

Extensive research has been conducted on thermal conductivity of various rock and mineral types. These are best reviewed by Eugene Robertson (1988) whose research is the main point of comparison of thermal conductivity research in this study. Mineralogy is the primary control for thermal conductivity in rock samples. Measurements typically are  $3.6 \text{ WM}^{-1}\text{K}^{-1}$  for calcite,  $5.5 \text{ WM}^{-1}\text{K}^{-1}$  for dolomite, and 2.0 for clays (Brigaud and Vasseu, 1989). Research by Thomas and Harvey (1973) found a different range with  $1.2 \text{ WM}^{-1}\text{K}^{-1}$  for porous chalk to  $5.1 \text{ WM}^{-1}\text{K}^{-1}$  for dolostone. Research by Naylor and Ellett (2014) found that Indiana glacier till ranges from  $1.6\text{--}1.8 \text{ WM}^{-1}\text{K}^{-1}$ . Bulk porosity is also main factor for different measurements reported by authors. Thermal conductivity generally decreases with increasing porosity due to water's lower thermal conductivity value (Robertson, 1988; Thomas and Harvey, 1973; Brigaud and Vasseu, 1989). Macroporosity can actually drastically raise thermal conductivity measurements in certain equipment due to water convection within pore space (Decagon Devices, personal communication).

## **2. Physical Setting of the Ball State University GCHP**

The nation's largest district-scale, whole-campus GCHP at Ball State University (BSU) is replacing aging coal-fired boilers (Lowe et al., 2010). The BSU project (3,600 BHEs) is dramatically larger—by more than a factor of four—than the campus-wide GCHP at Stockton College. Construction is in two phases with Phase I completed in 2011 and Phase II started in October 2011 (Figures 1,2). Phase I, located at the north end of the campus, consists of 1,800 double-loop BHEs drilled to a depth of 122 m and spaced 4.6 m. Phase II on the south end of campus will eventually comprise an additional 1,800 single-loop BHEs drilled to 153 m, also on

a 4.6 m spacing. All BHEs have a diameter of six inches and are completed with bentonite grout to the land surface. Drilling permits, borehole logs, and completion records are not required for BHEs since, as a closed system, they neither extract or inject fluid and, thus, do not meet the criteria of a well as defined within state and federal regulations (e.g., the Safe Drinking Water Act). However, the general contractor in Phase II has maintained completion records for each BHE.

BSU Facilities has provided exceptional access to system monitoring. Five nested monitoring wells were installed in Phase I alongside eight open wells installed into the shallow aquifer (Dunn, 2013). In Phase II, five nested monitoring wells are presently installed with an expectation of five additional nested wells by the end of construction east of the study area. In total BSU faculty, students, and collaborators will ultimately have access to 73 individual monitoring points surrounding and within the BHE fields at a range of depths (Dowling et al., In Review).

When complete, the BSU GCHP will contain two energy stations that simultaneously monitor the wells and produce the hot and chilled water necessary to heat and cool more than 45 major buildings that contain about 5.5 million square feet of air-conditioned space for the campus of ~22,000 students. Long-term expectations are to reduce the carbon footprint of the campus by approximately 50% and realize ~\$2 million in savings (Lowe et al., 2010). After two years, BSU has nearly achieved this goal, while only operating Phase I, by reducing CO<sub>2</sub> emissions by almost 50% or ~39,300 metric tons. Coal consumption has also dramatically reduced from more than 35,000 metric tons in 2008–2009 to ~1,500 metric tons in 2013–2014 (Lowe, oral communication, 2014). As of March, 2014, the coal burners were permanently taken off line and the building is undergoing conversion to natural gas.



## *2.1. Geology of East Central Indiana*

Few studies have been done on stratigraphy in the Muncie area and only The general stratigraphy of the area is known. Regional stratigraphy research in Delaware County has mainly been limited to Masters theses (Bloemker, 1981; Glasby, 1980; Owens, 1981). Measurements of formation thicknesses and facies analysis is restricted to locations of quarries and outcropping locations, the closest being the DeSoto quarry. Facies changes from type sections to the study area complicate well log correlations and lithological descriptions.

Glasby (1980) studied the Silurian bedrock geology by examining outcrops and quarries throughout the Muncie area. Of particular importance is her analysis of the Irving quarry in DeSoto. In ascending order is the Salamonie dolostone, Limberlost dolostone, Waldron formation, Louisville limestone, and Mississinewa Shale member of the Wabash formation. All are of the Niagaran series of the middle Silurian. The Salamonie is generally 7.6 m while the Limberlost averages 2 m Waldron 2 m and the Louisville is 20 m. The Mississinewa is 3m thick at the Buchanan quarry. Correlation between the Hoyt, Irving and Eaton quarries shows thinning towards the north.

Research by Bloemker (1981) focused on the Saluda member of the Whitewater formation. Bloemker notes that the Saluda changes significantly in lithology, paleontology, thickness, and stratigraphic relationships with adjacent formations. He proposed the Saluda Inter-tongueing within the Whitewater formation, which in previous research was directly below. The Saluda in the subsurface ranges from fine-grained dolostone to limestone. Principle lithologies are dolostone to calcareous dolostone. Inter-tongueing of Saluda in the Whitewater formation is seen in cores over 50 km apart. The Fort Atkinson Limestone of Illinois forms poorly defined tongues

in Eastern Indiana and is not mapped in detail (Gray, 1972). Scarpone (1997) identified approximately 7 m of shoal facies Fort Atkinson in Henry County south of Ball State University.

The Maquoketa group is approximately 220 m thick in Delaware County and does not outcrop in the Muncie area (Gray, 1972). Deep basin deposits (South West Indiana) consist entirely of shale. Upper lithology in the Eastern shelf is primarily limestone intertongued with gray shale. Regional correlations are mainly based off of geophysical well logs (gamma, resistivity). However, the intertonguing of the lithologic sequences greatly complicates the interpretation for the stratigraphy of the Maquoketa group.

## *2.2. Hydrology of East Central Indiana*

Surface geology throughout Indiana was formed by repeated Quaternary glaciations. Based on drilling and gamma logs, glacial till depth ranges from 6 m – 36 m and overlies the Silurian Pleasant Mills and Wabash formations. Glacial till is the thickest in the South West of the study area and shallows towards the Northeast. The majority of the ERT transects ran by Mundell et al. show that the glacier till is stratified with a thin (3 to 6 feet) layer of silt and clay overlying a thicker (6 to 9 feet) body of sand and gravel, under which lies a clayey layer of variable thickness (9 to 21 feet). Till is thicker in phase 2 and the ancestral Anderson river valley (Dunn, 2013).

ERT transects by Mundell and Associates predicted caves and karst features in the Silurian bedrock. Reports by drillers of lost circulation and sudden lowering of drilling string confirms this prediction. Samuelson et al. (2011)

## *2.3. Climate of East Central Indiana*

Ball State University in Muncie, Indiana has a hot and humid summer and a moderate winter. The Köppen climate classification of the study area is listed as humid subtropical (Peel et al. 2007). Average seasonal temperatures available from The National Climatic Data Center (NCDC - <http://www.ncdc.noaa.gov/oa/ncdc.html>) range from 24 °C in July to 0°C in January with summer maximum and winter minimum average temperatures of 30 °C and -5 °C, respectively. For 2011, the air maximum temperature was 36.1 °C and the lowest was 21.7 °C. Average monthly temperature during the study period ranged from -1.5 °C in January 2013 to 22.1 °C in July 2013. Total temperature ranged from 28.5 °C in August 2012 to -13.1 °C in January 2014.

Average regional annual precipitation in 2012 and 2013 was 90.6 cm and 106 cm respectively. Precipitation mostly occurs during winter and spring accounting for 60% of annual rainfall. Minimum precipitation in 2013 was 4.5 cm in February while greatest precipitation was 15.29 cm in April. Precipitation is primarily characterized by frontal systems entrained by Rossby waves and mesoscale convective events during the spring and early summer. During the summer and fall, comparatively more moisture from the Gulf of Mexico is entrained into these frontal systems than during the winter.

### **3. Methodology**

The research area comprises the eastern half of Phase 2 geothermal conversion project (Figure 1,2) on the Ball State University (BSU) campus. Five monitoring wells were drilled surrounding the area during the fall of 2012. Cuttings (Appendix 1) and borehole geophysical data from the research wells were used to develop a detailed understanding of the underlying geology (Figures 3-5). Drilling logs from borehole heat

exchangers (BHEs) combined with near-surface geophysical data were used to develop an understanding of the overlying glacial till and till-bedrock surface. Two bedrock cores from Delaware County north and northeast of the BSU campus provide additional context (Appendix 2) including measurements of the hydraulic and thermal conductivity of select stratigraphic intervals.

### *3.1. Electrical Resistivity Tomography*

During December of 2011, electrical resistivity transects in the Phase 2 field were collected in a cooperative agreement between Mundell & Associates, Inc. and BSU faculty and students to examine the composition of the glacial till and the bedrock stratigraphy and thickness. The surveys were conducted using an AGI Super String R8 with 56 electrodes configured in a dipole-dipole array. Seven transects were completed over a two day period). Transects 1-4 and 6 had an electrode spacing of five meters. Transect 5 had a spacing of 6 meters and transect 7 had a spacing of 4.5 meters. Transects 1 and 2 overlapped as well as transects 3 and 4. Earthimager 2D was used to compute inversions of the raw data (Mundell and Associates report in Appendix 3).

### *3.1. BHE Drilling Logs*

778 BHEs were drilled between January and August 2012 in Phase II of the geothermal conversion. Messer Inc., the general contractor for the drilling operations, provided completion logs for each BHE in PDF format (a digital archive of these completion logs is available upon request). Data for the depth to bedrock were extracted from each log. Contacts between rock types and formations were highly variable, were

inconsistently documented, and therefore considered inaccurate and not included in further analysis. Additionally, specific drill rigs noted bedrock contacts that were consistently higher or lower than neighboring rigs on parallel rows of BHEs. Some of these data were also eliminated to reduce the potential bias upon a final bedrock surface map. Using the natural neighbor and polynomial contouring algorithms in Surfer, two surface plots were generated of the contact between the Quaternary glacial till and the underlying Paleozoic bedrock (Figure 6).

### *3.2. Monitoring Well Logs and Cuttings*

Five nested monitoring wells were drilled associated with the Phase 2 field (Figure 2). Wells 2–5 were drilled around the perimeter of the field while Well 1 will ultimately be in the middle of the field once Phase 2 is completed in 2014. The author observed drilling operations conducted by Helvie and Sons, Inc. from Marion, IN during September to November 2012. The contractors used a mud rotary top head drive Indersol Rand TH-60 drilling rig. Cuttings of rock were collected from the returned drilling mud in composite increments of ten feet of drill stem. The lag time between cutting production at the drill bit and recovery from the returned drilling mud was not considered during sample collecting.

Samples were cleaned in the lab and the petrology analyzed with a binocular microscope. The lithology was determined using 5% HCl to distinguish between carbonate and siliciclastic material and Alizarin Red to discriminate between limestone and dolomite. Texture, including grain size, sorting, and rounding (if practical), was characterized using the Dunham classification system for carbonate fabric (Dunham,

1964). Identifiable fossils, sedimentary structures, and secondary mineralization (e.g., pyrite) were also recorded. The collected information was archived in MPlot software from Mudlogging Systems, Inc.

### *3.3. Borehole Gamma, Resistivity, and Spontaneous Potential*

Borehole gamma was collected from each of the five monitoring wells during the winter of 2013 in collaboration with Marni Karaffa of the Indiana Geological Survey and using a Matrix Logging System with a 2PGS-1000 PolyGamma Probe in R and SP mode. Resistivity and spontaneous potential data from Well 3 were also acquired. These geophysical data were used to correlate formation data between wells, identify the contact between the glacial till and bedrock, and aid in interpretation of logged rock cuttings from the monitoring wells. Gamma data was most importantly used for correlating well cuttings to appropriate depths, but were not available for Well 5, which is consequently not considered in the remainder of this research. Data was collected every 0.05m, but in the effort to eliminate background noise and prevent in over interpretation of data, only data on the interval of 0.3048 m (1ft) is considered. The stratigraphic columns for each monitoring well produced from the combined cutting and gamma data are archived in Appendix 1.

### *3.4. Bedrock Cores*

Two bedrock cores drilled in Delaware County were examined at the core repository archive of the Indiana Geological Survey in Bloomington, IN (Appendix 2). Cores SDH 236 collected in 1973 from the Muncie Stone Company 16.2 km Northeast of

Ball State University (NAD 83 UTM 16S 639102 E, 4466670 N and B-1 collected in 1964 from the Irving Brothers Quarry 8.7 km northeast of Ball State University (NAD 83 UTM 16S 0641974 E, 04455990 N) were examined using a binocular microscope and a standard hand lens. Core logs were constructed for both cores on an interval of 0.3048 m (1ft) using carbonate log sheets modified from those provided by Bebout and Loucks (1984) and utilized by Florea (2006) (Appendix 2). Methods to determine lithology and texture match that of the cuttings. Additional information included relative quantification of pore type and size, relative induration, fossil type and abundance, sedimentary structures, and secondary alterations and mineralization.

### *3.5. Matrix Permeability and Porosity*

Eight samples at key stratigraphic intervals (3.0 m, 12.0 m, 14.0 m, 22.0 m, 28.0 m, 32.0 m, 39.0 m, 53.0 m, 58.0 m, 62.0 m) distributed among the geologic formations and representative facies types were taken from B-1 core to test for values of matrix permeability. Core Labs in Houston made the measurements using a steady-state micropermeameter (Core Labs report in Appendix 4). For each sample, 2.54 cm-diameter plugs were drilled from each sample perpendicular to the core direction. Thus, the measurements are representative of horizontal permeability and no sense of anisotropy at the matrix scale could be determined.

Values of bulk porosity were determined by comparing the volume of pore spaces in the sample, measured by the change in weight between dry samples and those same samples after vacuum saturation with water, to the volume of the sample, measured by water displacement in a graduated cylinder to an estimated accuracy of  $\pm 5$  mL.

### *3.6. Thermal Conductivity*

Fourteen samples (3.0 m, 8.2 m, 10.4 m, 12.2 m, 14.3 m, 21.6 m, 23.8 m, 28.4 m, 35.4 m, 39.0 m, 48.8 m, 53.0 m, 57.9 m, 62.2 m) were selected from the B-1 core to test for values of dry and water-saturated thermal conductivity (photos in Appendix 3). Measurements were collected at the Indiana Geological Survey using a KD2 Sensor by Decagon Devices, Inc. with a RK-1 rock sensor package. Samples were generally selected based on formation type and facies relationships within the core; however, equipment restrictions guided the selection of specific samples. For each sample, a 6.8 mm hole was drilled and filled with thermal grease. Heating experiments with the thermal probe were replicated three times for each sample. The measurement time was ten minutes for each run. A second set of triplicate measurements were collected on the same set of samples after vacuum saturation with water. Thermal conductivity ( $\text{W m}^{-1} \text{K}^{-1}$ ), final temperature (C), and error values were recorded along with the arithmetic mean and standard deviation for each set of measurements (Tables 1-3).

## **4. Results**

### *Summary Paragraph*

The data from this study reveal a complicated karstified bedrock surface beneath a glacial till aquifer that ranges from 10–30 m. The underlying Paleozoic bedrock comprises near-horizontal layers of dolostone, limestone, and shale dating from the Late Silurian and early Ordovician periods. These formations thicken slightly towards the southwest. Facies range from mudstone through grainstone and have matrix



permeabilities ranging between  $10^{-17}$  and  $10^{-14}$  m<sup>2</sup>. Matrix permeability and porosity are highest in the Silurian grainstones and vuggy limestones. Thermal conductivity dry samples ranges between  $1.55 \text{ WM}^{-1}\text{K}^{-1}$  to  $3.32 \text{ WM}^{-1}\text{K}^{-1}$  with a linear relationship between dry and wet measurements of conductivity.

#### *4.1. Pre-glacial bedrock surface and glacial stratigraphy*

The inversions of the ERT data in EarthImager 2D reveal a complex bedrock surface with an overburden of glacial till (Appendix 3). Modeled resistivity values in Lines 1 and 2 are mostly less than  $100 \text{ } \Omega\text{-m}$  (Appendix 3), significantly lower than in the other transects and suggesting influence from the metal fence that parallels the path of this transect. Resistivity values in the remaining transects are more typical of glacial till and carbonate rocks saturated with water and largely range between  $100\text{--}1000 \text{ } \Omega\text{-m}$  (Appendix 3). Lower values in these transects are consistent with soil or layers of silt or clay. The bedrock contact undulates and is generally at a greater depth toward the east and south (Figure 6). A nearly continuous layer of higher resistivity material centered at approximately 10 m in depth likely marks a sand and gravel zone within the glacial till.

The BHE drill logs identify the sand and gravel zone in the glacial till as a ‘chatter zone’. These logs also record the complexity of the bedrock topography throughout the research area (Figure 6). The natural neighbor and polynomial contouring algorithms reveal quite different results. The natural neighbor algorithm preserves the integrity of original data (Figure 6) and results in an irregular contour plot suggesting a pre-glacial bedrock surface with depressions and rock pinnacles in the bedrock. Inaccuracies in drillers logs and actual bedrock topography is sometimes difficult to distinguish; however,

as data is highly dependent on driller log accuracy. The local polynomial contouring method results in considerable smoothing of the data and shows a gentle trend toward deeper bedrock contacts towards the southeast (Figure 6). Drill logs and gamma data from the monitoring wells support this thickening trend (Appendix 1, Figures 4,5), with Well 3 (the southeast well) having the greatest overburden of till.

#### *4.2. Bedrock stratigraphy and structure*

The combination of gamma data, cuttings from monitoring wells, and core logs were used to develop the stratigraphic column for the study area (Figure 3). In all wells, Silurian-age limestone, dolostone, and shale of the Salina Group overly the Ordovician-age limestone and shale of the Maquoketa Group. Rock unit nomenclature fits the stratigraphic organizations outlined by Gray (1972) and research in Henry County from Scarpone (1997). Peaks in the gamma data coincide with soil and clay in the overburden and organic-rich shale in the bedrock, such as within the Cataract Formation and Brainard Shale. Lowest gamma values occur at depths comprised of pure carbonate material, such as in portions of the Pleasant Mills and Salamonie Limestone. Strong deflections in the gamma data occur at the contact between the glacial till and the bedrock and at stratigraphic contacts within the bedrock, which are summarized in Appendix 3.

Most formation boundaries have sharp contacts, both in core and in the gamma data (Figure 3). For example, the contact between the glacial till and the Salina Group and the contact between the Salina and Maquoketa Groups represent significant disconformities in the sedimentary record. The topography on the pre-glacial bedrock surface is considerable, such that cuttings consistent with 6.5 m of dolostone from the Mississinewa

Shale member of the Wabash Formation are only seen in Well 1. Cuttings from all other wells start in the Pleasant Mills.

Carbonate rocks of the Salina Group are visually similar in texture, grain size, facies, and fabric (Appendix 1,2). They alternate in centimeter to decimeter cycles between a packstone and a sucrosic grainstone with medium to coarse texture. Stringers of wackestone are also present in the more argillaceous portions of the Waldron, Salamonie, and Cataract Formations. The transition between the Salamonie and Cataract Formations is a gradational boundary comprised of chert lenses, limestone, and shale stringers that are more easily identified in core and not in the cuttings. These shale lenses are too thin to show up as individual gamma spikes, rather there is a relatively strong shift in gamma readings across this formational boundary (Appendix 1, Figure 3-5)

The mixed carbonate and siliciclastics of the upper Ordovician Maquoketa Group have a wide range of texture, grain size, facies, and fabric (Appendix 1). For example, the upper Whitewater Formation is largely a well-indurated, fossil-rich, moldic limestone. Some molds include significant secondary mineralization such as pyrite. The lower Whitewater Formation, in contrast becomes more argillaceous. The Saluda inter-tongues within the Whitewater and is a partially dolomitized argillaceous limestone. The Ordovician Brainard Shale and Dillsboro Limestone both consist of centimeter to decimeter cycles of limestone and shale. These cycles are reflected in the rapidly changing gamma data. Cyclicity continues with a loss of carbonate into the Kope Formation at the base of the sedimentary sequence in our wells.

Formations contacts reveal a slight dip toward the northeast. Well 2 and Well 4 have the shallowest and deepest formation contacts, respectively (Figure 3,4). The

Salamonie through Kope formation tops in the north to south transect (wells 4 & 3, Figure 4) and west to east transect (wells 1–3, Figure 5) reveal averaged formation apparent dip angles towards the north and east of  $0.76^{\circ}$  and  $0.34^{\circ}$ , respectively. There is little variation in dip angle from each formation and averaged true dip angle and dip direction are computed as  $1.1^{\circ}$  to the NNE at  $25.4^{\circ}$ . Table 4 provides a summary of the apparent and true dip angles for each stratigraphic contact.

#### *4.2. Hydrostratigraphy*

Values of matrix permeability are summarized in Table 5 and with a range from  $< 9.9 \times 10^{-17} \text{ m}^2$  in the lowermost Waldron Formation to  $2.2 \times 10^{-14} \text{ m}^2$  in the lowermost Cataract Formation. Matrix permeability generally decreases with increased siliciclastics. Despite the small sample size ( $n = 8$ ), there is some relationship between matrix permeability and facies. For example, the highest matrix permeability in the Salamonie Formation,  $2.2 \times 10^{-16} \text{ m}^2$ , is from a poorly washed grainstone and the lowest matrix permeability,  $< 9.9 \times 10^{-17} \text{ m}^2$ , is from a wakestone. In the Fort Atkinson, the sample of poorly washed, but well indurated, grainstone at 52.7 m has a matrix permeability of  $7.9 \times 10^{-16} \text{ m}^2$  compared to the mudstone–packstone facies at 57.9 m with matrix permeability of  $3.1 \times 10^{-15} \text{ m}^2$ .

Porosity changes with depth are summarized in Tables 1 and 6 as well as Figure 7. Similar to matrix permeability, values follow facies changes. For example, samples of grainstones that are sucrosic dolomites at 10.4 m in the Pleasant Mills Formation and 21.6 m in the Salamonie Formation show unusually high porosity values of 14.4% and 15.7%, respectively. In contrast, shale from the Waldron Formation, the Cataract

Formation, and the Brainard Shale have porosities that range between 2.8% and 4.8%. Values in the vuggy limestones of the Whitewater Formation range between 8.2% and 9.4%.

#### *4.3. Thermal stratigraphy*

Average dry thermal conductivity readings range between  $1.5 \text{ WM}^{-1}\text{K}^{-1}$  in the lower Waldron Formation to  $3.3 \text{ Wm}^{-1}\text{K}^{-1}$  in the Fort Atkinson Limestone (Tables 1,2) with standard deviations range between 0.006 and  $0.086 \text{ WM}^{-1}\text{K}^{-1}$ . There is no trend in values with depth, but there is some correlation with facies—carbonates are more conductive to heat, on average, than shale.

Water saturated samples show greater thermal conductivity than the equivalent dry samples (Tables 1-3, Figures 7-9). The standard deviation of these water-saturated samples is also greater, most particularly in the upper Pleasant Mills and Fort Atkinson samples, where water convection may impact the stability of the measurement. Figure 10 illustrates the average value of saturated thermal conductivity versus the equivalent measurement in the dry sample. A relatively good linear relationship is seen between dry and wet ( $r^2 = 0.905$ ) with water saturated samples 2.3 times more conductive than the equivalent dry sample.

### **5. Discussion**

Research and design of GCHP systems are typically conducted using “black box” methods that assume a homogeneous lithology without groundwater flow—the standard thermal response test (TRT). This includes the GCHP system being constructed at BSU.

An unresolved question beyond the scope of this thesis is whether TRTs give an accurate representation of system response to thermal loading in a layered sedimentary aquifer with groundwater flow, particularly in a large field of BHEs where interference or buoyant convection may play a significant role in the structure of the thermal plume.

Within the GCHP system at BSU, comprising more than 3,000 BHEs, heat capacity will not be spatially consistent. Pinch outs, lateral facies changes, and changes in formation thicknesses do occur. Although the general stratigraphy of bedrock at Ball State University has been known for some time, a more detailed knowledge aids in understanding the nature of subsurface capacity to store and transport thermal energy. Therefore, the mission of this thesis is simple, to provide a detailed petro-physical study of the stratigraphy beneath BSU that will serve as a foundation for future investigations.

### *5.1 Surficial and Glacial Geology*

The surface geology of BSU and the greater east-central Indiana region are the product of repeated phases of Quaternary glaciation. Remnants of the most recent glacial phase comprise lateral and end-moraine features as well as thick glacial till. Based on the drilling and ERT data collected thus far (Appendix 3), the glacial till ranges between 15 and 46 m thick, and overlies a bedrock surface marked by an irregular epikarst. Drilling, gamma, and ERT data also reveal that the glacial till is stratified, with at least one significant horizon of gravel and boulders wedged between finer grained units and centered at approximately 10 m in depth (Appendix 3).

The thickness of the glacial changes over short distances within and around the study area. The natural-neighbor map of drilling depths to bedrock illustrates the potential irregularity of the bedrock surface from karst processes. In contrast, the local polynomial map of Figure 6

emphasizes overall trends in bedrock surface. Both maps show thickening towards the southeast. Previous research (Samuelson, unpublished data) illustrates that this area is adjacent to the buried valley of the ancestral Anderson River.

The thickness of glacial till is the single most variable characteristic in the lithology of BHEs in this study. This could have a profound impact on the bulk hydraulic and thermal conductivities in each BHE. For example, BHEs drilled in the southwest corner of Phase 2 closer to Well 3 have approximately 37 m of glacial till (23% of the borehole depth). In contrast, Wells 1 and 4 include 30 m of glacial till that comprises only 18% of the BHE. In Dunn (2013), the thickness of glacial till in Phase 1 is even less (between 10 m and 20 m). Although thermal conductivity measurements for glacial till have not been collected in this study, clay loam and glacial till have a conductivity that ranges between  $2.14 \text{ WM}^{-1}\text{K}^{-1}$  –  $2.5 \text{ WM}^{-1}\text{K}^{-1}$  (Shawn Naylor, personal communication; Casas et al., 2013; Clauser and Huenges, 1995); values that are lower on average than for carbonate rocks (Robertson, 1988).

Thus, BHEs with a large fraction of glacial till, such as those in the southeast part of the Phase 2 field, may have reduced thermal capacities than that those BHEs with smaller fractions of glacial till. On the other hand, BHEs in the northwestern part of the Phase 2 field may have greater thermal capacities due to reduced thickness of glacial till and the presence of the Mississinewa Shale Member of the Wabash Formation (Pinsak and Shaver, 1961; Owens, 1981) and potential presence of an overlying micritic dolostone facies (Droste and Shaver, 1983) (Appendix 1, 2).

## *5.2. Ordovician–Silurian Stratigraphy of East-Central Indiana*

Gamma, core, and well logs from this study illustrate the range of lithologies in

east-central Indiana and the differences from the type sections (Shaver and others, 1961; Gray, 1972; Brown and Lineback, 1966). This difference between type section and local lithology makes estimating the petro-physical properties difficult and rationalizes a detailed investigation. Since carbonate content is directly related to thermal conductivity (Robertson, 1988), formation composition has direct implications for the thermal capacity of the GCHP system.

Cavernous porosity, identified by bit drops and loss of circulation during drilling operations, is common within the Silurian strata, particularly in the north field of Phase 1. Unlike the extensive paleokarst encountered at the Ohio State GCHP (Bair and Torres, 2011) the ‘caves’ under BSU may be related to the active circulation of shallow groundwater adjacent to the ancestral Anderson River prior to mantling by glacial till. So far in Phase 2, BSU students collecting data alongside drilling rigs have only encountered a few signatures of these caves but the ERT data and drilling logs displays possible evidence of sinkholes on the pre-glacial surface (Appendix 3, Figures 4,5).

In one example, the Waldron Formation becomes more calcitic further southeast from the type section (NE¼ sec. 6, T. 11 N., R. 8 E at the abandoned Standard Materials Corp. quarry) towards the north and west (Elrod, 1883; Pinsak and Shaver, 1964; Shaver and others, 1961). Pinsak and Shaver (1964) used the name Waldron for dominantly dolomitic facies in northern Indiana and the core analysis near BSU shows shale laminae disseminated within a dense argillaceous dolostone. The Indiana Geological Survey reintroduced the Waldron as a member of the Pleasant Mills formation in northern Indiana, but were not able to account for thickly interbedded, gradational sequences of Waldon–Pleasant Mills in some places (IGS Compendium, 1984).



The presence of the Fort Atkinson Limestone was not unexpected due to research from Scarpone (1997). His close research, in Henry County, however, described the Fort Atkinson as lobes of uncertain thickness with pinchouts in the area. The Fort Atkinson may very well be absent in other areas in or around Delaware county which would greatly change the vertical section stratigraphy.

The thickness of the glacial changes over short distances within and around the study area. The natural-neighbor map of drilling depths to bedrock in Figure 6 emphasizes a true fit to drillers logs and illustrates the potential irregularity of the bedrock surface from karst processes. In contrast, the local polynomial map emphasizes overall trends in bedrock surface. Both maps show thickening towards the southeast. Previous research (Samuelson, unpublished data) illustrates that this area is adjacent to the buried valley of the ancestral Anderson River.

ERT transects (Appendix 3) and drilling logs (Appendix 1) illustrate that the thickness of glacial till is the single most variable characteristic in BHE lithology. This would have a profound impact on the bulk hydraulic and thermal conductivities in each BHE. BHEs drilled in the southwest corner of Phase 2 closer to well 3 have approximately 37 m of glacial till (23% of borehole). Wells 1 and 4 with 30 m of glacial till comprise only 18% of the BHE. In Dunn (2013), the thickness of glacial till in Phase 1 is even less (between 10 m and 20 m). The wells in phase 1 are drilled to a shallower depth at 122m compared to 152m for phase 2. Even though the wells are drilled shallower, the total thermal transfer ability may be larger in phase 1 than in phase 2.

Clays have an insulating effect on thermal conductivity (Casas et al., 2013, Robertson, 1988). Although thermal conductivity measurements for downhole glacial till

have not been collected in this study, clay loam and glacial till have a conductivity that ranges between  $2.14 \text{ Wm}^{-1}\text{K}^{-1}$  –  $2.5 \text{ Wm}^{-1}\text{K}^{-1}$  (Ellet and Naylor, 2014; Casas, 2013, Clauser, 1995). Since thermal conductivity is driven by mineralogical properties, claystone and shales have similar thermal conductivity values at  $2.0 \text{ Wm}^{-1}\text{K}^{-1}$  (saturated) and have very similar thermal characteristics (Casas et al., 2013; Robertson, 1988).

Thus, BHEs with a large fraction of glacial till, such as those in the southeast part of the Phase 2 field, should have lower total thermal capacities than that those BHEs with smaller fractions of glacial till. In contrast, BHEs in the northwestern part of the Phase 2 field may have greater thermal capacities due to reduced thickness of glacial till and the presence of the Mississinewa Shale Member of the Wabash Formation (Pinsak and Shaver, 1964) and potential presence of an overlying micritic dolostone facies (Droste and Shaver, 1983) (Appendix 1). Future gamma and cuttings data from the western half of Phase 2 should confirm the existence of the Wabash Formation in that area.

### *5.3. Thermal Conductivity Measurements vs. Standard Thermal Tests*

Measured values of thermal conductivity (Table 1,2,3) generally agree with previous research by Eugene Robertson (1988). Robertson's measurements from samples of pure carbonate crystals yield slightly higher conductivity values, but measured values in this study are within his range of reported lithological and mixed lithology values. Other factors not seen in samples (secondary porosity, karstification, and stress fields) will also most likely lead to higher thermal capacities (Sass and Gotz, 2012). A direct comparison of measured values to that of Robertson (1988) is not entirely applicable due the mixed lithology of samples utilized, but is a good benchmark of comparison.

Petrographic research was not utilized on the tested samples because the core used for research is 8.7km away from the study area and may not completely reflect complete similarity to the stratigraphy at BSU. Therefore, it is not possible to directly compare the carbonate/clay ratio to conductivity. Samples, however, are in line with that of Robertson (1988) with more argillaceous carbonate samples having lower thermal conductivity values and the distance of the samples from the research area is not considered to be a problem.

This mixed lithology and facies greatly complicate thermal conductivity both vertically through each individual BHE and laterally through Phase II. The addition of clay minerals lowers the measurements of thermal conductivity in limestone and dolostones as expected from Brigaud and Vasseur (1989). Values of conductivity in the Ordovician samples follow this trend (Figures 7,8). In addition, air and water play a role in lowering measured thermal conductivity, although in different proportions. Stringers of shale in the lower Salamonie Formation, the mixed lithology of the Cataract Formation, and the clay within the Whitewater and Dillsboro Formation are all examples of irregular lithologies that both yield lower thermal conductivity and complicate measurements within each respective formation. Since the formation boundary of the Dillsboro and Kope is often arbitrarily picked off of clay content (Gray, H., 1972), the boundary may be very different in phase 1 and phase 2.

Increase between dry and saturated samples at first look erratic (Figure 9). When dry and saturated values are compared against each other, a strong linear relationship is seen where saturated values are 2.28 times higher than dry values (Figure 9). This is due from the replacement of air with water. Both air and water have low thermal conductivity

values (0.025 and 0.5 respectively). This illustrates the great effect water has on thermal conductivity. Values fall within two distinct groups within this figure. The group with lower values all hold significant amounts of clay mud. Values from the group with higher thermal conductivity are all grainstone facies or have much lower clay content. This effect is similar to that seen in Brigaud and Vasseur (1989) and Robertson (1988) where increasing clay content logarithmically decreases thermal conductivity of sandstones.

Measured thermal conductivity in the Whitewater at 57.4 m and 62.7 m are much higher than maximum values from Robertson (1988). Porosity is relatively low to moderate at 4.3% and 8.2% respectively and the matrix permeability is within range of other samples. It is very likely that the RK-1 probe was drilled into at least one rock void. Although methods may have been responsible for these high values, it is more likely that they are due to water convection within the sample pores. Water not only has a higher conductivity than air, but thermal loading induces water convection within the pores themselves and thus significantly raises heat transfer and heat movement throughout formation. This however does not suggest that thermal loading on a large scale will force water convection within and across formations.

The methodology used to measure thermal conductivity with the RK-1 probe is new and unfortunately there are no publications to compare results, or methodology. Thus there is some speculation on what exactly is causing the high values (Decagon, personal communication). This effect is not seen on the Whitewater sample at 67 m. Even though it has a high porosity at 9.4%, it also has a relatively high clay content and small pore spaces that would lower or eliminate this effect.

#### *5.4. Hydraulic Conductivity and Porosity vs. Existing Hydrogeology Data*

Cardinal Creek dominates the surface hydrology at BSU. It drains a storm-water retention pond and then flows between the BHE fields in Phase 1 (Figure 1). Fluid resistivity data from the monitoring well in Phase 2 illustrates the decreased influence of meteoric water with depth and subdivides the groundwater environment into five stratigraphic zones: a surficial glacial aquifer, an unconfined Silurian aquifer (Pleasant Mills Formation), an upper leaky aquitard (Waldron Formation), a semi-confined Silurian aquifer (Salamonie and Cataract Formations), a lower aquitard (Brainard Shale), and the confined Ordovician aquifer (Whitewater, Dillsboro, and Kope Formations) (Figure 3).

The direction of groundwater flow in the shallow glacial aquifer and the Silurian aquifer is generally toward the southwest in Phase 1 (Samuelson, et al., 2011; Dunn, 2013). Similar groundwater flow data is not yet available for Phase 2. Results of slug tests in monitoring wells in the Silurian and the surficial glacial aquifer from Phase 1 reveal permeability values between  $1.7 \times 10^{-13} \text{ m}^2$  and  $2.7 \times 10^{-13} \text{ m}^2$  (Dunn, 2013) and are considerably greater than the matrix permeability measurements of this study— $< 9.9 \times 10^{-17} \text{ m}^2$  in the lowermost Waldron Formation to  $2.2 \times 10^{-15} \text{ m}^2$  in the lowermost Cataract Formation. This highlights the importance of bedding planes and fractures in groundwater movement (Pentecost and Samuelson, 1978). Similar data is not yet available for the Ordovician aquifer.

Recent slug tests by Dunn (2013) have a high standard deviation in hydraulic conductivity measurements, but are considerably higher than matrix permeability values measured (Table 5). Values range from  $8.65509 \times 10^{-8} \text{ (m/s)}$  in the upper Silurian aquifer to  $8.23148 \times 10^{-6} \text{ (m/s)}$  in the lower Silurian aquifer (Dunn, 2013). Matrix permeability measurements from Core Labs (Table 5) are generally low, but do range on orders of

magnitude within and across formations. The only possible way this could occur is if the majority of local groundwater flow is through joints, bedding planes, and fractures. Research by Samuelson (1976) showed oriented fractures and joints close to BSU along the Kankakee arch. Local bedrock fractures may be following this pattern.

There is no correlation between measured permeability in this study and thermal plume development measured from Dunn (2013). It is assumed that zones of higher permeability would transfer more heat due through groundwater flow. Measured groundwater temperature probably reflects average data across formations. The eight data points are not enough to show the overall trend.

Matrix permeability of the eight samples measured is linked to lithology and facies. Silurian grainstones have matrix permeability an order of magnitude higher than that of the packstones (Table 1). Since the alternation of grainstones and packstones is seen on the centimeter scale in both the Irving Bros. and Muncie stone Co. cores, lateral groundwater flow in the Silurian strata is complicated through a pattern of alternating high and low zones of permeability. Horizontal heat transfer through groundwater movement in these strata should follow facies changes.

Matrix permeability measurements were conducted on different samples than thermal conductivity and porosity measurements. Comparison between the two is difficult because lithology type and characteristics change on a small scale. Even though samples were in close proximity in core (95% extraction), exact characteristics are not guaranteed. Sass and Gotz (2012) has cited this persistent problem for research in the geothermal field and stress the importance of all measurements on the same samples. For example, siliclastic mud changes small-scale lithology in the Cataract and Whitewater

and Silurian facies changes on the centimeter scale. The general trend, however, is still apparent. Silurian dolostones overall have higher permeability which is seen in slug tests and temperature data from Dunn (2013).

Porosity does not at first seem to affect thermal conductivity values of rock samples. It was expected that higher porosity values would lead to higher thermal conductivity values due to pore water convection. This effect is seen in the upper Whitewater sample and interestingly the single Ft Atkinson sample (Figure 10). Pore water convection may not only be due to bulk porosity, but also the type of porosity. Macrovugular rock facies (parts of the Whitewater) may have more pore convection than samples with similar bulk porosity. Porosity does not seem to control thermal conductivity in shale dominated samples (Figure 11). Mean saturated conductivity is similar in the Cataract, Waldron, Brainard, and upper Salamonie (Figure 11) over a porosity range of 2.8%–15.7%. Mean saturated thermal conductivity for these samples ranges from 1.79K–2.84K which is consistent with previous research.

The remaining samples may show strong relationship with thermal conductivity. With pure carbonate lithology, the three Silurian grainstones show strong control of saturated conductivity through a small change in porosity.

### *5.5. Predicting Groundwater Temperature Changes and Comparing to Existing Data*

It is clear that in comparing lithology, thermal conductivity, and permeability/porosity to groundwater temperature changes from Dunn (2013) that shale content directly affects groundwater temperature. Glacier till, Brainard formation, and the Kope shale all show lessened responses from thermal loading.

Current groundwater thermal data shows stratified warming through formations. Zones of higher permeability and thermal conductivity should be reflected in zones of higher groundwater temperature. Data from the M2 well (Dunn, 2013) supports this with zones of higher rates of groundwater warming in the Pleasant Mills, Waldron, and Salamonie dolostones (20-40m) (Fig 7). The Cataract Dolostone (dirties downwards) shows a decrease in groundwater temperature down formation. The sample at 39m (Tables 1,5) is of very high permeability for a formation with significant clay content. Two possibilities can be considered 1) Core labs mistyped the permeability measurement 2) The eight samples taken out of the 204' of core is not representative of the core itself.

The Brainard and Kope shales (70m and 110m) can be seen in dips of temperature reflecting shale's low thermal and hydraulic conductivities. The Whitewater and Dillsboro limestones can both be seen with groundwater temperature slowly and then rapidly decreasing. This corresponds to the increasing shale content in the Ordovician limestones.

#### *5.6. Thermofacies*

Ferguson (2007) considered the effects of horizontal heterogeneity in aquifer hydraulic conductivity on temperature distributions and energy recovery by injecting and pumping groundwater from virtual wells. This work utilized geostatistical simulations to generate virtual aquifers based on characteristics of the well-studied Borden sand aquifer in Ontario and the paleokarstic Carbonate Rock aquifer in Manitoba. The results showed that the effect of heterogeneity was to spread heat over greater distances in the aquifer.



At BSU, Dunn (2013) summarized the temperature changes in the groundwater at the active Phase 1. As of October 2013, after constant thermal loading, a temperature increase of 14–18 °C was been observed in the center of the south BHE field in Phase 1 (Dunn, 2013) with concurrent increases in three other monitoring wells. Three of the monitoring wells with increased temperatures overall also exhibit vertical structure in the temperature profiles that may correlate to stratigraphic units—the thermofacies of Sass and Götz (2012). A temperature ‘spike’ at a depth between 14–19.5 m may correspond to the sand and gravel zone of the surficial glacial aquifer (Figure 3) and a temperature ‘dip’ at a depth of 70 m agrees with the position of the Brainard shale aquitard (Figure 3), zones of higher permeability and lower thermal conductivity, respectively.

This vertical heterogeneity in temperature profiles are reminiscent of models of pump-and-treat remediation systems (Vacher et al., 2006): high heat transfer at first, followed by reduced efficiency as water flowing in from more permeable layers becomes responsible for most heat transfer and less permeable regions become isolated. The results have similarity to the models developed in MODFLOW and MT3D 96 by Vacher et al. (2006) where the variation in bulk permeability of the Ocala Limestone in Florida was utilized to demonstrate the heterogeneous penetration of a tracer during injection cycles of ASR wells in the Upper Floridan aquifer. Rest periods would lead to ‘rebound’ when temperature equilibrium is re-established between low and high permeability zones.

## **6. Conclusions**

In June of 2011, Geothermal Resource Technologies, Inc. conducted a pair of standard TRTs in Phase 2 of the BSU GCHP. The results of these two tests concluded a bulk ‘formation’

thermal conductivity between 2.6 and 3.0  $\text{WM}^{-1}\text{K}^{-1}$ . The average thermal conductivity from samples in this study, not weighted for formation thickness, was 2.2 and 3.5  $\text{WM}^{-1}\text{K}^{-1}$  for dry and water saturated samples, respectively. Importantly, due to core availability, our data do not include the shale-rich Brainard (shale facies), Dillsboro and Kope Formations, which comprise a significant proportion of lower thermal conductivity media in each BHEs. The range in our thermal conductivity data from saturated samples (1.8–7.2  $\text{WM}^{-1}\text{K}^{-1}$ ) leads the logical conclusion that the TRTs do not capture where the heat is stored and recovered or how the heat is transported.

Our research provides some insight with support from preliminary temperature profiles in an active portion of the GCHP. First, zones of low siliciclastics within the Silurian Salamonie Limestone and moldic porosity within the Ordovician Fort Atkinson Formation may be target thermofacies for heat deposition and extraction. Sand and gravel zones within the glacial till may also allow for significant thermal loading. Advection along groundwater flow paths in these high-permeability zones may reduce the fraction of this heat that is recoverable; however this may be a nonissue since BSU is a cooling dominant system. Portions of the unconfined Silurian aquifer may also be subject to significant thermal advection where paleokarst features increase aquifer permeability and influence groundwater flow. Characterization of the hydrogeologic environment can therefore be a vital tool for district-scale GCHPs by allowing system designers to tune the field of BHEs to the specific on-site conditions that may influence the magnitude and mode of heat transfer.

## References

- Abdulagatov, I., Emirov, S., Abdulagatova, Z., Askerov, S., 2006, Effect of Pressure and Temperature on the Thermal Conductivity of Rocks: *Journal of Chemical Engineering*, v. 51, no. 1, p. 22-33.
- Abdulagatova, Z. Z., Abdulagatov, I. M., & Emirov, V. N. 2009,. Effect of temperature and pressure on the thermal conductivity of sandstone: *International Journal Of Rock Mechanics And Mining Sciences*, v. 46, no, 6, p. 1055-1071.
- Armitage, D., Bacon, D., Massey-Norton, J., Miller, J., 1980, *Ground-Water Heat Pumps: An Examination of Hydrogeologic, Environmental, Legal, and Economic Factors Affecting Their Use*: U.S. Department of Energy, DOE/CS/20060-5120.
- Bloemker, J., Subsurface stratigraphy and pelecology of the Saluda formation (upper Ordovician) of Indiana (M.S. thesis): Ball State University, 105 p.
- Bair, E.S., Torres, M., 2011, Problems drilling and completing geothermal wells in a paleokarst terrain: *Geological Society of America Abstracts with Programs*, v. 43, no. 5, p. 167.
- Banks, D. 2008, *An Introduction to Thermogeology: Ground Source Heating and Cooling*. Blackwell Publishing, Ltd, Oxford.
- Brigaud, F., and Vasseur, G., 1989, Mineralogy, porosity, and fluid control on thermal conductivity of sedimentary rocks: *Geophysical Journal*, v. 98, no. 3, p. 525-542.
- Brown, G. D., Jr., and Lineback, J. A., 1966, Lithostratigraphy of Cincinnati Series (Upper Ordovician) In southeastern Indiana: *American Association of Petroleum Geologists Bulletin*, v. 50, p. 1018-1023.
- Casas, L., Pozo, M., Gomez, C., Pozo, E., Bessieres, L., Plantier, F., Legido, J., 2013, Thermal behavior of mixtures of bentonitic clay and saline solutions: *Applied Clay Science*, v., 72, p. 18-25.
- Curtis, R., Lund, J., Sanner, B., Rybach, L. Hellström, G. 2005, Ground source heat pumps—geothermal energy for anyone, anywhere: Current worldwide activity. *Proceedings World Geothermal Congress*, Turkey.
- Diao, N., Qinyun, L., Fang, Z., 2004, Heat transfer in ground heat exchangers with groundwater advection: *International Journal of Thermal Sciences*, v. 23, p. 1203-1211.
- Droste, J. B., and Shaver, R. H., 1983, *Atlas of early and middle Paleozoic paleogeography of the southern Great Lakes area*: Indiana Geological Survey Special Report, vol. 32, 32 p.
- Dunham, R. J., 1962, Classification of carbonate rocks according to depositional textures: *Memoir – American Association of Petroleum Geologists*, p. 108-121

- Dunn, M.E., 2013. Effects of Gound-Coupled Heat Pumps on Hydrogeologic Systems: Ball State University. MS Thesis, Ball State University, Muncie, 86 p.
- Dunn, M., Dowling, C.B., Florea, L.J., Neumann, K., Samuelson, A. 2012. Evaluating temporal and thermal variations in hydrogeologic data at Ball State University's ground-source geothermal system (Muncie, IN). *Geological Society of America Abstracts with Programs* 44(5): 22.
- Elrod, M. N., 1883, Geology of Decatur County: Indiana Department of Geology and Natural History Annual Report. V. 12, p. 100-152.
- Epstein, C. 1998, Impact of groundwater flow on the Stockton geothermal well field, *in* Proceedings of the Second Stockton International Geothermal Conference, New Jersey.
- Epstein, C. Sowers, L., 2006, The continued warming of the Stockton geothermal well field, Ecstock, *in* Proceedings of the Tenth Stockton International Geothermal Conference, New Jersey.
- Epstein, C., Skinner, W., Stiles, L., Taylor, H., Sowers, L., Pal, S., 1996, Geothermal heating on a very large scale: the Stockton College Facility: *Well Water Journal*, v. 9, no. 3, p. 38-41.
- Ferguson, G., 2007, Heterogeneity and thermal modeling of ground water: *Ground Water*, v. 45, no, 4, p. 485-490.
- Florea, L.J. 2006. The Karst of West-Central Florida (Ph.D. diss): University of South Florida, Tampa.
- Freedman, V., Waichler. S., Mackley, R., Horner. J., 2012, Assessing the thermal environmental impacts of an groundwater heat pump in southeastern Washington State: *Geothermics*, v. 42, p. 65-77.
- Geothermal Map. n.d. Ball State University, accessed 12 January 2012, <http://cms.bsu.edu/About/Geothermal/FAQ/GeothermalMap.aspx>.
- Glasby, V., Silurian bedrock geology of the Muncie area (M.S. thesis): Ball State University, 54 p.
- Gotz, A., and Sass, I., 2012, Geothermal reservoir characterization: a thermofacies Concept: *Terra Nova*, v. 24, no. 2, p. 142-147.
- Gray, H., 1972, Lithostratigraphy of the Maquoketa group (Ordovician) in Indiana, Special Report no. 7.
- Helmke, M.F., Gatlin, D., Cuprak, G., Wilson, R.B., Alderson, H., Babcock., N., 2013, Performance of a large geoexchange system in fractured gneiss of Southeast

- Pennsylvania: Geological Society of America Abstracts with Programs, vol. 45, no. 7, p.858.
- Lowe, J., Koester, R. Sachtleben, P., 2010, Chapter 17: Embracing the Future: The Ball State University Geothermal Project in Universities and Climate Change: Introducing Climate Change to University Programmes (ed W.L. Filho), Springer-Verlag, Berlin, DOI 10.1007/978-3-642-10751-1\_17.
- Lund, J., Sanner, B., Rybach, L., Curtis, R., Hellström, G., 2004, Geothermal (Ground-Source) Heat Pumps: A World Overview: GHC Bulletin, v. 25, p. 1-10.
- Markel, J.M., Schincariol, R.A., 2007, Thermal plume transport from sand and gravel pits: Potential thermal impacts on cool water streams: Journal of Hydrology v. 338, no. 3-4, p. 174-195.
- Mundell and Associates, 2009, Geophysical investigation of Ball State MEP geothermal project Muncie, Indiana (M09005) Indianapolis, IN: Mundell and Associates.
- Mundell, J. A., and Hebert, G. J. 2010, Geophysical imaging to enhance analysis, design and drilling of large-scale geothermal systems, *in* Proceedings Of SAGEEP, p. 845-851.
- Owens, R., 1981, Petrologic analysis of the Mississinewa member of the Wabash formation and the effect of reef proximity on interreef sedimentation (M.S. thesis): Ball State University, 82 p.
- Peel, Murray C., Brian L. Finlayson, and Thomas A. McMahon., 2007, Updated world map of the Köppen-Geiger climate classification: Hydrology and earth system sciences discussions vol. 4, no. 2, p. 439-473.
- Pentecost, D. C., & Samuelson, A. C. 1978, Fracture Study of the Paleozoic Bedrock in East Central Indiana, *in* Proceedings of the Indiana Academy of Science, vol. 88, p. 263-277.
- Pertzborn, A., Nellis, G., Klein, S., 2011, Impact of weather variation on ground-source heat pump design: HVAC&R Research, p. 174-185.
- Pinsak, A. P., and Shaver, R. H., 1964, The Silurian formations of northern Indiana: Indiana Geol. Survey Bulletin, vol. 32, 87 p.
- Raymond, J., Therien, R., Gosselin, Borehole temperature evolution during thermal response tests: Geothermics, v. 40, p. 69-78.
- Robertson, E., 1988, Thermal properties of rocks: U.S. Geological Survey Open-File Report 88-441.
- Rybach, L. Eugster, W.J., 2002, Sustainability aspects of geothermal heat pumps *in* Proceedings: twenty-seventh workshop on geothermal reservoir engineering, Stanford University, CA.

- Samuelson, A., Dowling, C., Neumann, K., Bonneau, P., 2011, Baseline Hydrogeological characteristics of the first phase ground-Source geothermal field at Ball State University (Muncie, IN): 32<sup>nd</sup> Annual Indiana Water Resources Association Conference.
- Sanner, B., Karytsas, C., Mendrinos, D., Rybach, L., 2003, Current status of ground source heat pumps and underground thermal energy storage in Europe: *Geothermics*, v. 32, p. 579–588.
- Scarpone, G., The subsurface geology of the Fort Atkinson formation in Indiana (M.S. thesis): Ball State University, 97 p.
- Schlueter, E., Zimmerman, R., Witherspoon, P., Cook, N., 1997, The fractal dimension of pores in sedimentary rocks and its influence on permeability: *Engineering Geology*, v. 48, p. 199-215.
- Shaver, R. H., Ault, C. H., Burger, A. M., Carr, D. D., Droste, J. B., Eggert, D. L., & ... Wier, C. E., 1986, Compendium of Paleozoic rock-unit stratigraphy in Indiana; a revision. Geological Survey Bulletin Bloomington, Ind., no. 59.
- Shaver, R. H., and Others, 1961, Stratigraphy of the Silurian rocks of northern Indiana: Indiana Geological Survey Field Conference. Guidebook 10, 62 p.
- Siliski, A., 2014, Petro-physical characterization of the geology underlying Phase 2 of the Ball State University geothermal conversion (M.S. Thesis): Ball State University, Muncie.
- Siliski, A., Florea, L.J., Dowling, C.B., Neumann, K., Samuelson, A.C., 2013, Geophysical and petrophysical characterization of the Ball State University geothermal conversion: *Geological Society of America Abstracts with Programs*, v. 45, no. 7, p. 774.
- Taylor, H., Stiles, L., Hemphill, W., 1998, Technical description of the Stockton College geothermal HVAC retrofit, *in* Proceedings of the Second Stockton International Geothermal Conference, New Jersey.
- Tester, J.W., Drake, E.M., Golay, M.W., Driscoll, M.J., Peters, W.A., 2005, Sustainable Energy—Choosing Among Options. MIT Press, Cambridge, MA.
- Tester, J.W., Anderson, B.J., Batchelor, A.S., Blackwell, D.D., DiPippo, R., Drake, E.M., Garnish, J., Livesay, B., Moore, M.C., Nichols, K., Petty, S., Toksoz, M.N., Veatch, R.W., Baria, R., Augustine, C., Murphy, E., Negaru, P., Richards, M., 2000. The Future of Geothermal Energy: MIT Press, Cambridge, MA.
- Thomas, J., Frost, R., Richard, H., 1973, Thermal conductivity of carbonate rocks: *Engineering Geology*, v. 7, p. 3-12.
- Vacher, H.L., Hutchings, W.C., Budd, D.A., 2006, Metaphors and models: The ASR bubble in the Floridan Aquifer: *Ground Water*, v. 44, no. 2, p. 144–154.

Witte, H.J.L., van Gelder, A.J., Klep, P., 2006, A very large distributed ground source heat pump project for domestic heating: Schoenmakershoek, Etten-Leur (The Netherlands), Ecstock, *in* Proceedings of the Tenth Stockton International Geothermal Conference, New Jersey.

Zierfuss, H., and Vliet, G., 1956, Laboratory measurements of heat conductivity of sedimentary rocks: Bulletin of the American Association of Petroleum Geologists, v. 40, no. 10, p. 2475-2488.

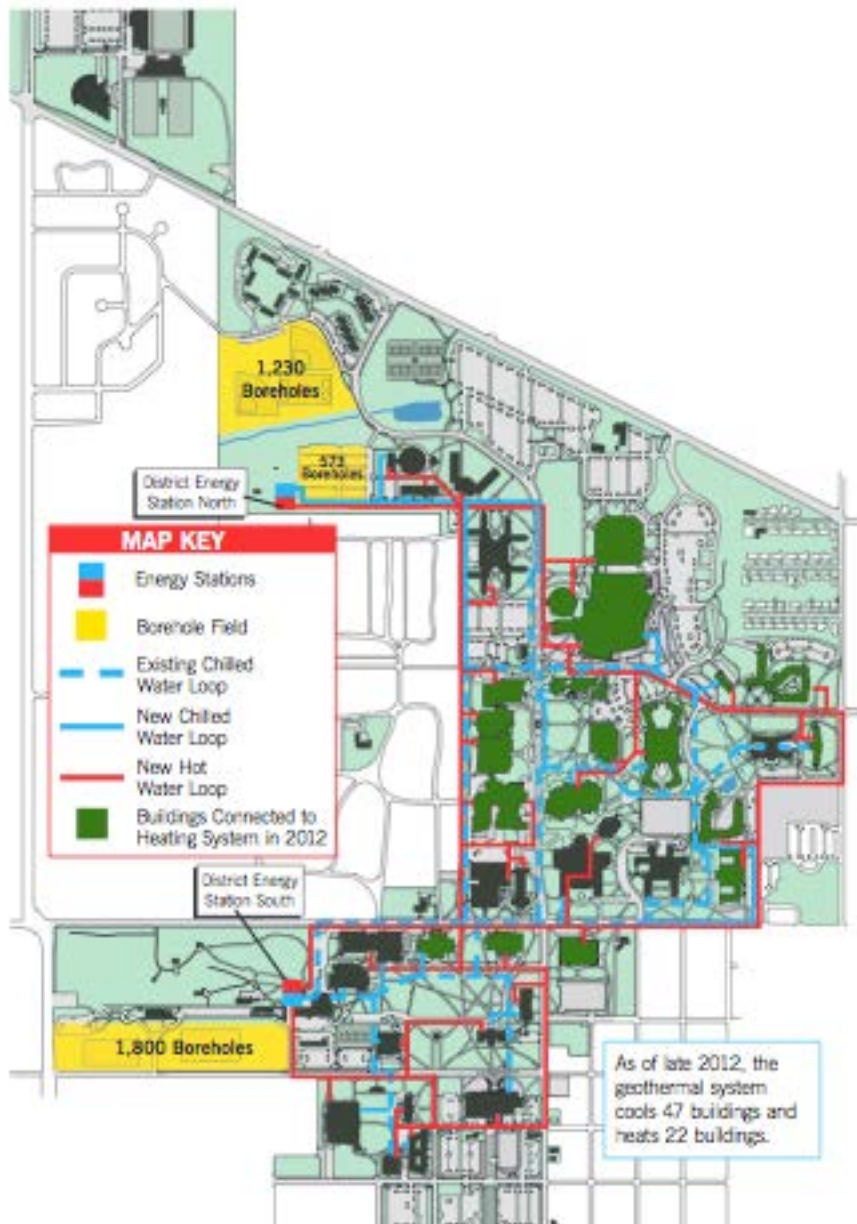


**Figure 1: Map of the Ball State University Geothermal System**



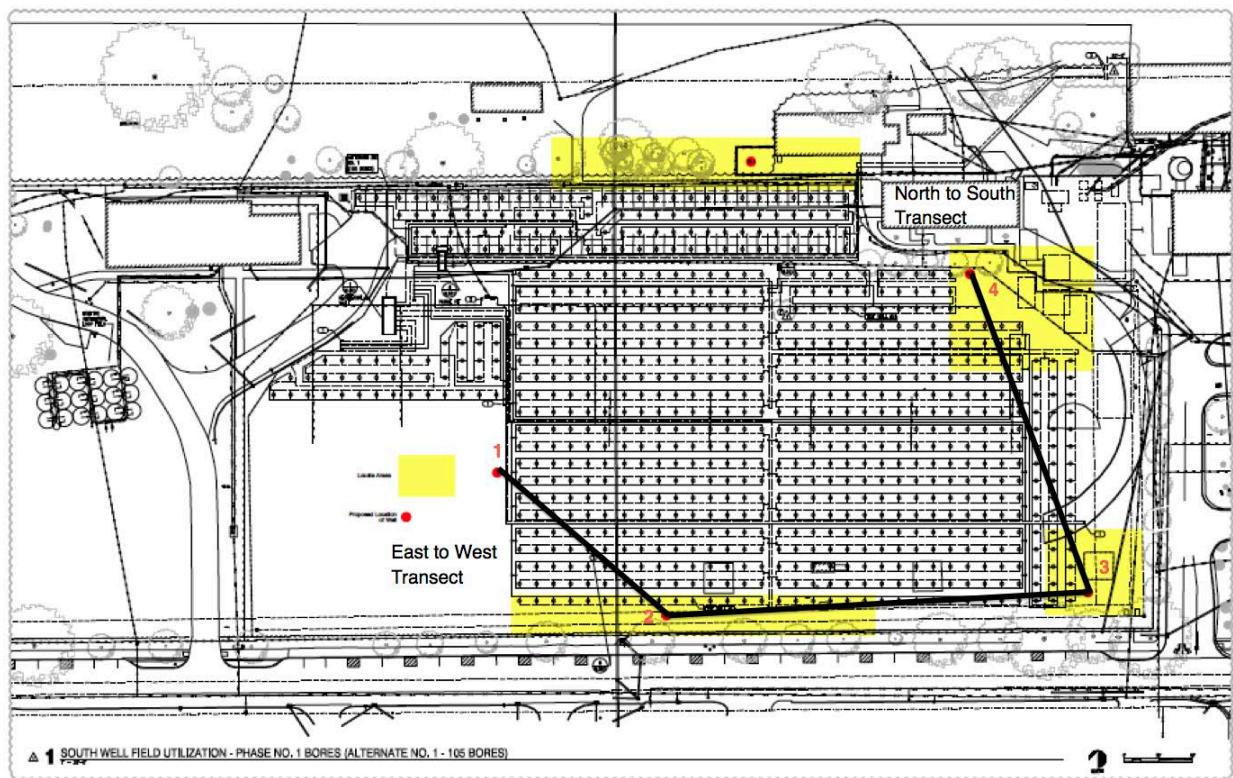


**Figure 2: Map of the Study Area**

# Composite Stratigraphic Column

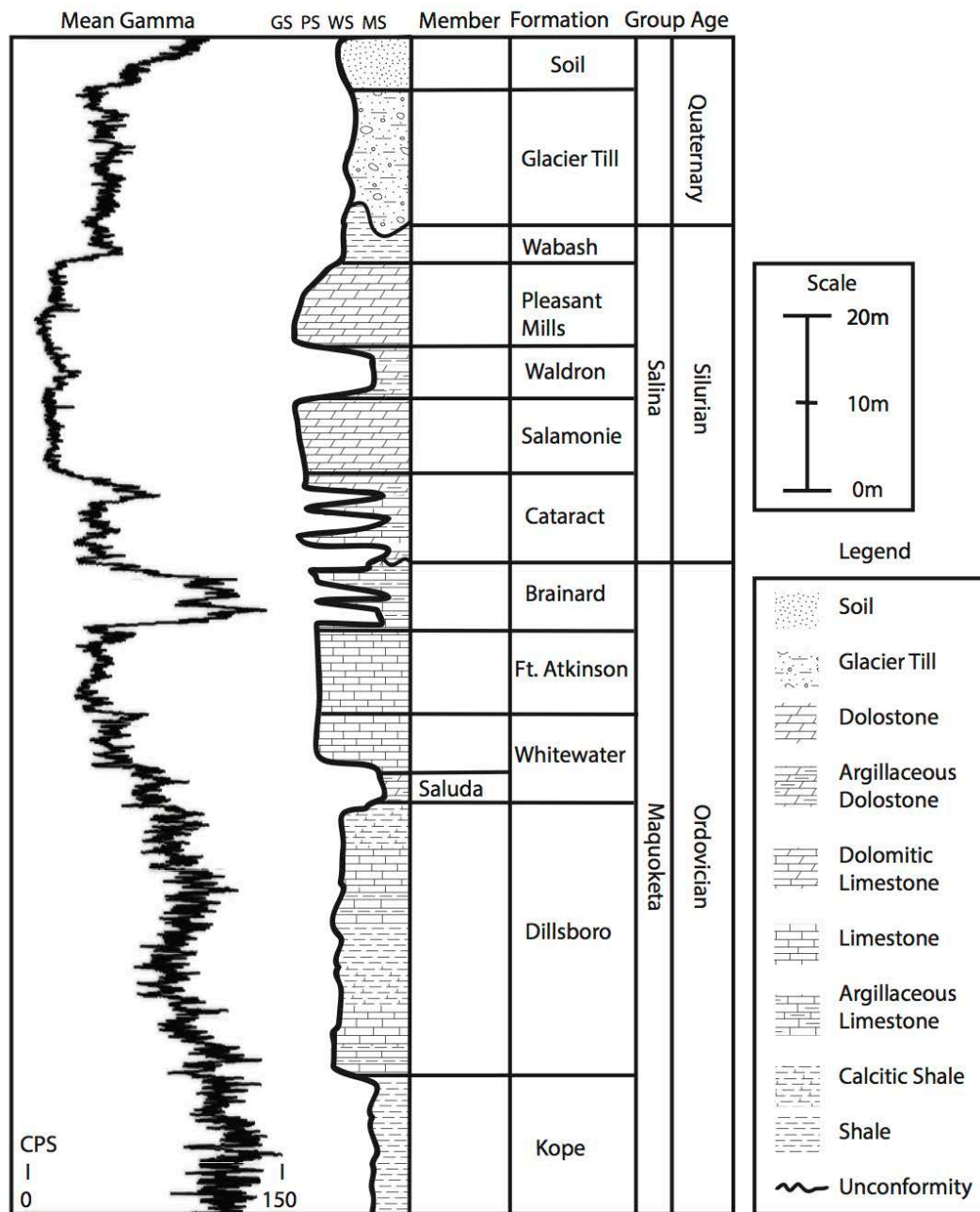
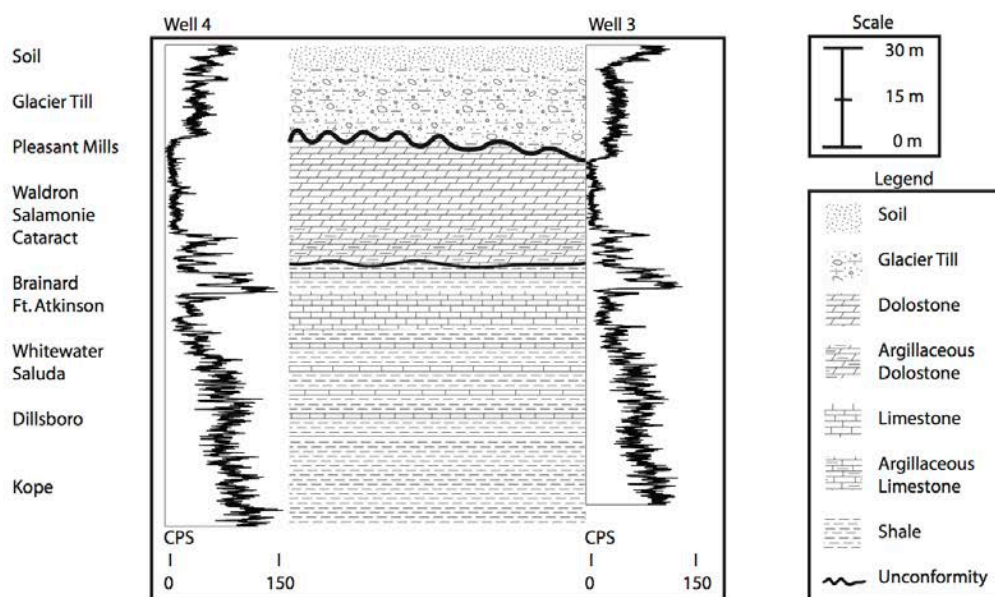


Figure 3: Composite Stratigraphy Column of Study Wells 1-4

# North to South Transect



**Figure 4: N-S Transect of Study Area**

# West to East Transect

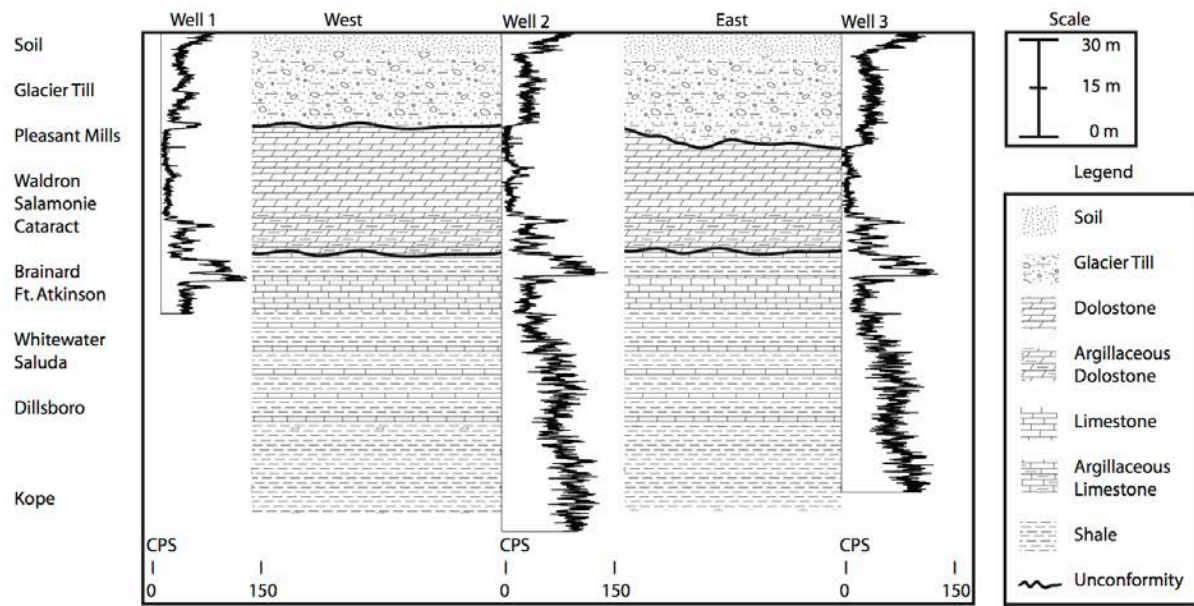


**Figure 5: W-E Transect of Study Area**



# Topographic Maps of Research Area

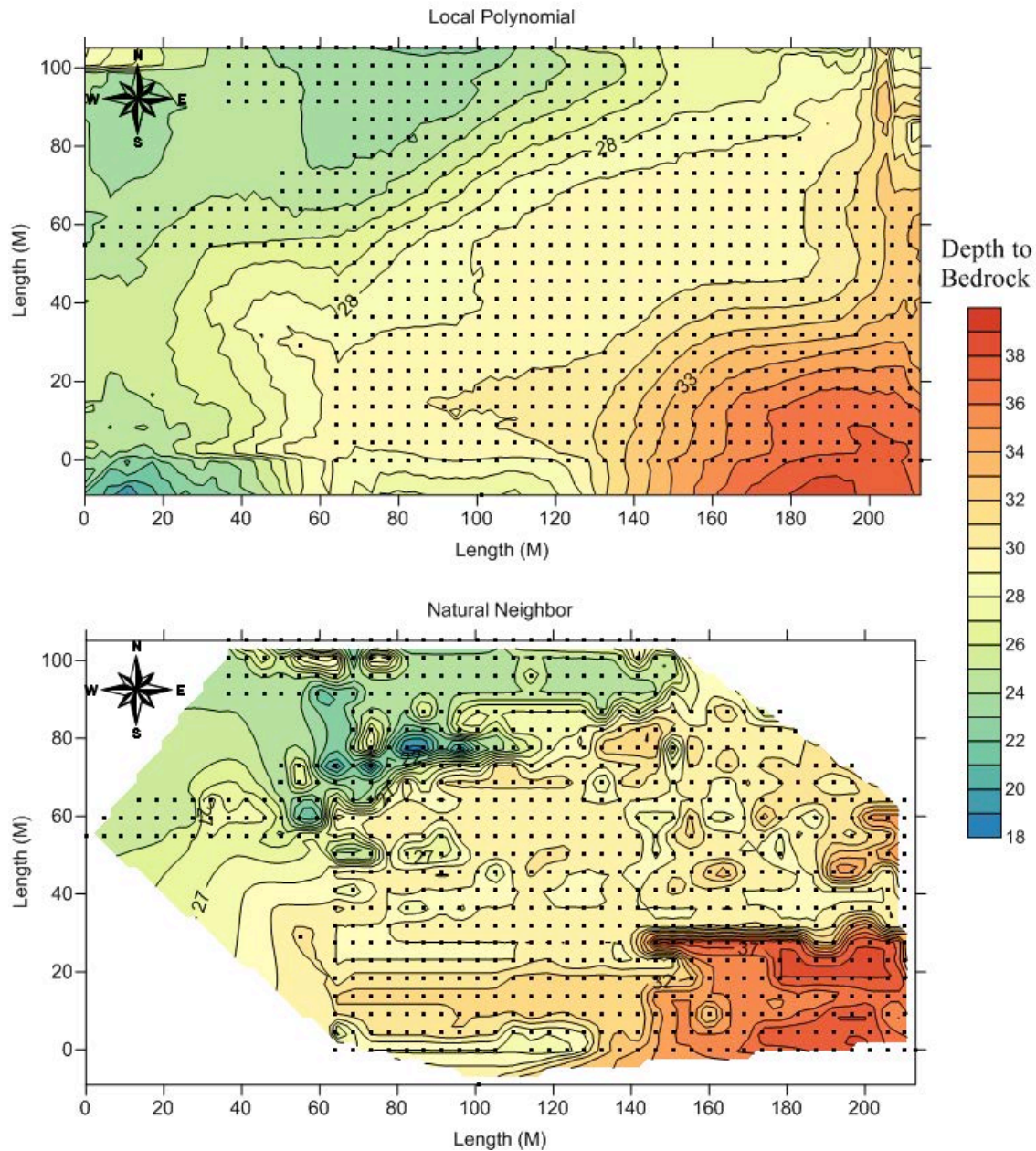


**Figure 6: Depth to Bedrock Map of Study Area**

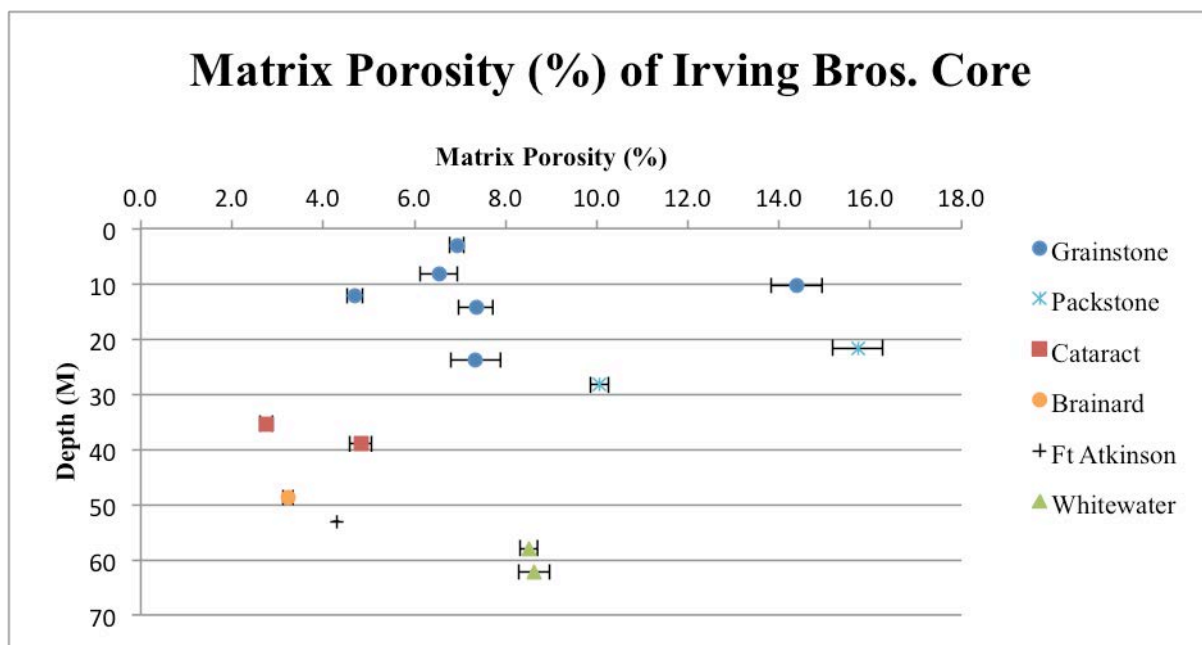


Figure 7: Porosity vs. Depth of the Irving Bros. Core

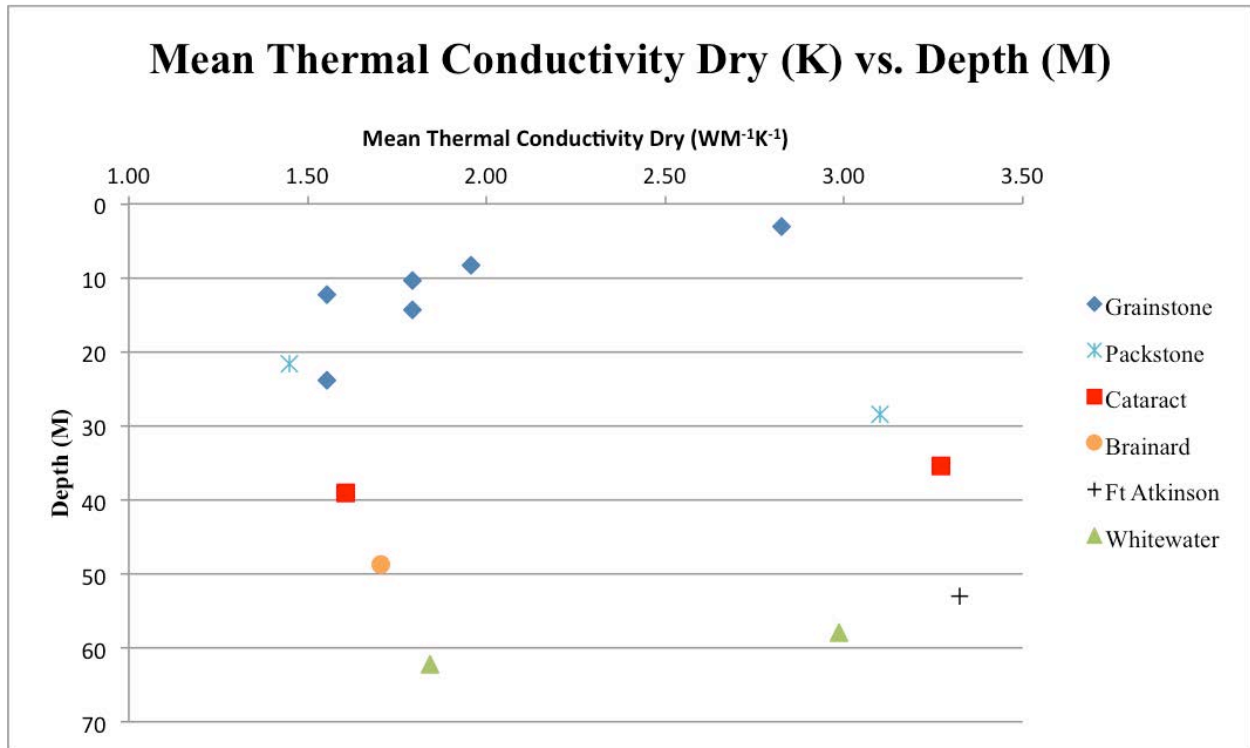
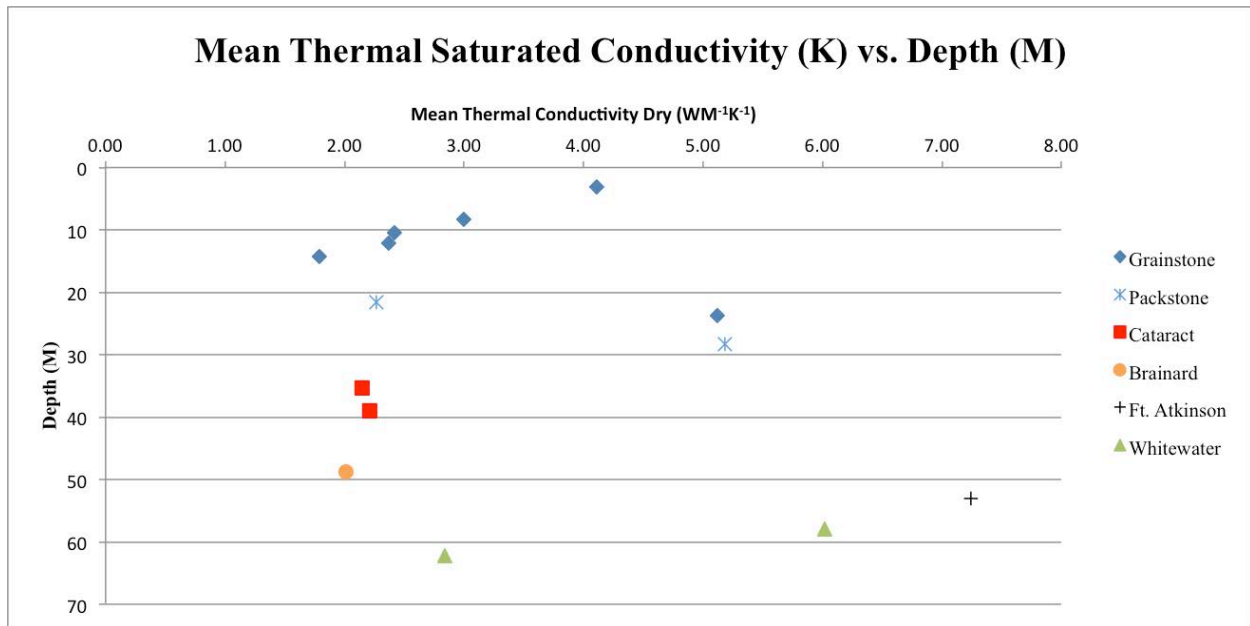


Figure 8: Mean Thermal Conductivity Dry vs. Depth of the Irving Bros. Core



**Fig 9: Mean Thermal Conductivity Saturated vs. Depth of the Irving Bros. Core**



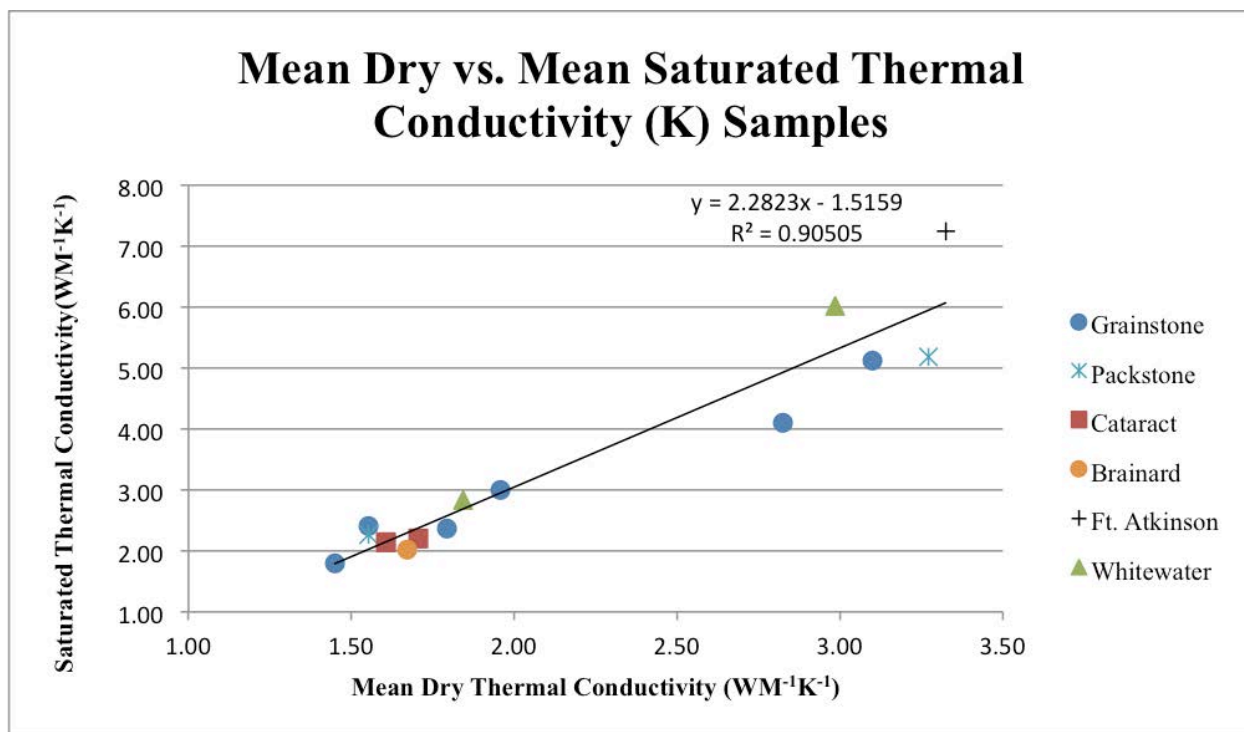
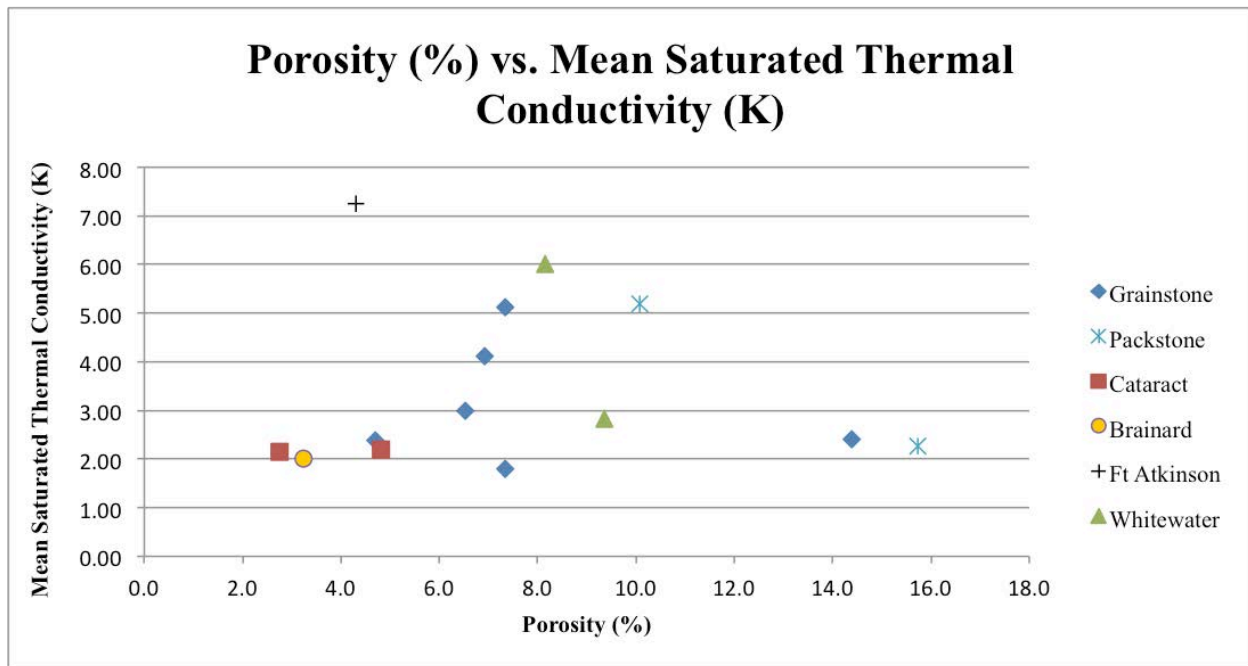


Figure 10: Mean vs. Saturated Thermal Conductivity of the Irving Bros. Core



**Figure 11: Bulk Porosity vs. Mean Saturated Thermal Conductivity of the Irving Bros. Core**

Table 1: Summary						
Depth	Formation	Mineralogy	Matrix Porosity	Matrix Permeability	Mean Dry K	Mean Saturated K
(M)			(%)	(M <sup>2</sup> )	(WM <sup>-1</sup> K <sup>-1</sup> )	(WM <sup>-1</sup> K <sup>-1</sup> )
3.0	Pleasant Mills	Dolostone	<b>0.100</b>	1.49E-15	2.83	4.11
8.2	Pleasant Mills	Dolostone			1.96	3.00
10.4	Pleasant Mills	Dolostone			1.55	2.42
12.2	Waldron	Argillaceous Dolostone			1.79	2.37
14.3	Waldron	Argillaceous Dolostone	<b>0.120</b>	<9.87E-17	1.45	1.79
21.6	Salamonie	Dolostone			1.55	2.27
21.9	Salamonie	Dolostone	<b>0.216</b>	3.53E-15		
23.8	Salamonie	Dolostone			3.10	5.12
28.3	Salamonie	Dolostone	<b>0.127</b>	2.15E-16	3.27	5.18
32.0	Salamonie	Dolostone	<b>0.103</b>	1.92E-15		
35.4	Cataract	Limestone, Dolostone, Shale			1.61	2.14
39.0	Cataract	Limestone, Dolostone, Shale	<b>0.115</b>	2.19E-14	1.70	2.21
48.8	Brainard	Shale, Limestone			1.67	2.01
52.7	Whitewater	Shale, Limestone	<b>0.094</b>	7.94E-16		
53.0	Whitewater	Shale, Limestone			3.32	7.24
57.9	Whitewater	Shale, Limestone	<b>0.098</b>	3.06E-15	2.99	6.02
62.2	Whitewater	Shale, Limestone			1.84	2.84

<b>Table 2: Mean Dry Thermal Conductivity of Irving Bros. Core</b>					
<b>Depth (M)</b>	<b>Formation</b>	<b>K(WM<sup>-1</sup>K<sup>-1</sup>)</b>	<b>T (°C)</b>	<b>Error (%)</b>	<b>StDev</b>
3.0	Pleasant Mills	2.83	21.02	0.02	0.07
8.2	Pleasant Mills	1.96	21.19	0.03	0.01
10.4	Pleasant Mills	1.55	20.79	0.02	0.04
12.2	Waldron	1.79	20.98	0.02	0.03
14.3	Waldron	1.45	21.26	0.03	0.04
21.6	Salamonie	1.55	20.94	0.02	0.01
23.8	Salamonie	3.10	20.95	0.02	0.05
28.3	Salamonie	3.27	21.01	0.02	0.02
35.4	Cataract	1.61	20.99	0.02	0.01
39.0	Cataract	1.70	21.06	0.02	0.02
48.8	Brainard	1.67	21.30	0.02	0.02
53.0	Ft Atkinson	3.32	21.39	0.03	0.08
57.9	Whitewater	2.99	21.01	0.02	0.09
62.2	Whitewater	1.84	21.81	0.02	0.05

<b>Table 3: Mean Saturated Thermal Conductivity of Irving Bros. Core</b>					
<b>Depth (M)</b>	<b>Formation</b>	<b>K(WM<sup>-1</sup>K<sup>-1</sup>)</b>	<b>T (°C)</b>	<b>Error (%)</b>	<b>StDev</b>
3.0	Pleasant Mills	4.11	18.88	0.03	1.51
8.2	Pleasant Mills	3.00	18.86	0.05	0.80
10.4	Pleasant Mills	2.42	18.89	0.03	0.66
12.2	Waldron	2.37	18.36	0.05	0.09
14.3	Waldron	1.79	18.56	0.03	0.30
21.6	Salamonie	2.27	18.48	0.03	0.43
23.8	Salamonie	5.12	18.39	0.03	0.36
28.3	Salamonie	5.18	18.44	0.03	0.53
35.4	Cataract	2.14	18.33	0.03	0.55
39.0	Cataract	2.21	18.25	0.02	0.35
48.8	Brainard	2.01	18.27	0.03	0.07
53.0	Ft Atkinson	7.24	18.33	0.05	1.19
57.9	Whitewater	6.02	18.25	0.04	2.90
62.2	Whitewater	2.84	17.90	0.04	0.43

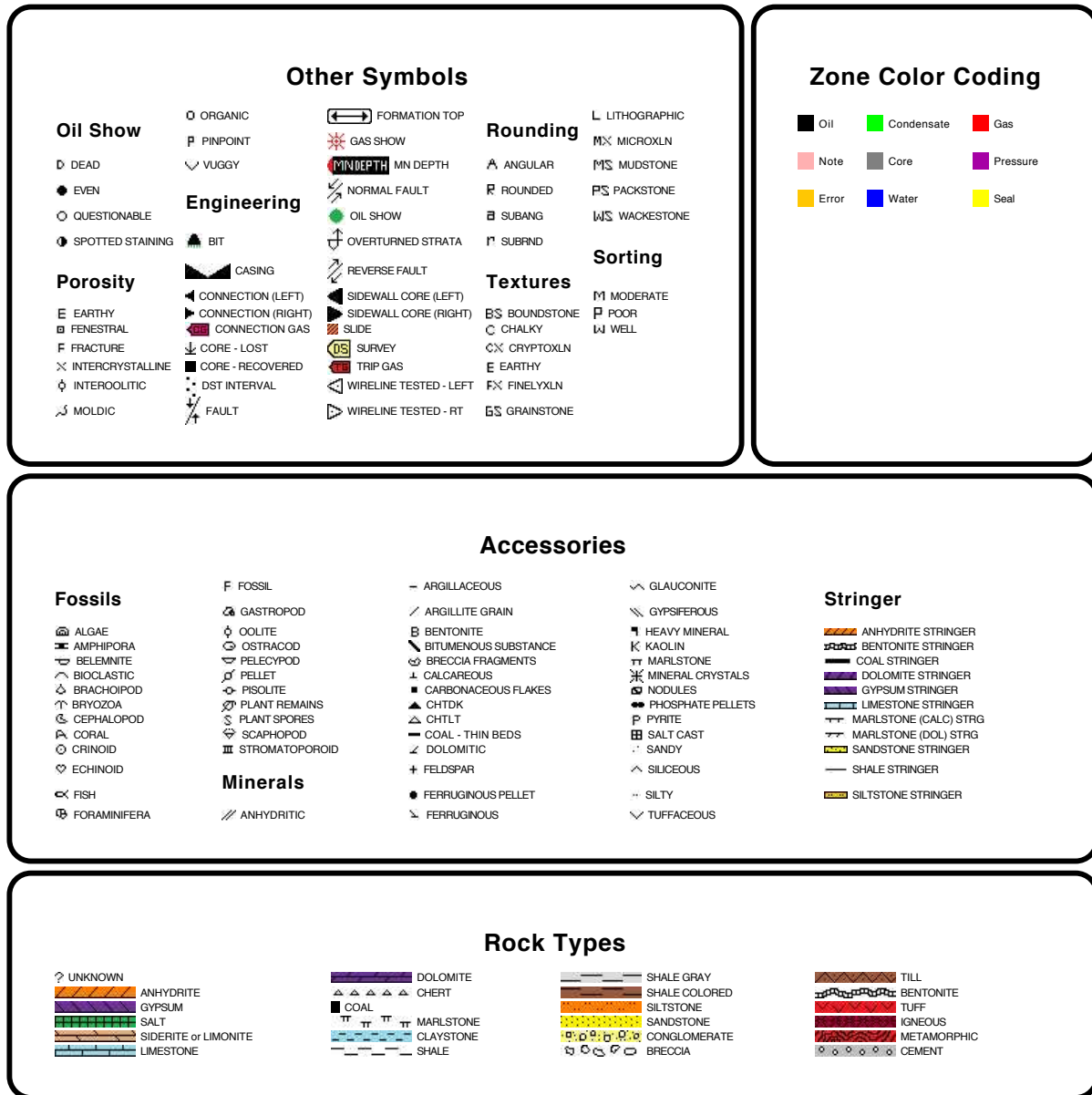
<b>Table 4: Bedrock Dip and Dip Direction of Research Area</b>			
<b>Formation</b>	<b>Wells 1-3</b>	<b>Wells 3-4</b>	<b>TRUE</b>
Waldron	0.59	0.46	0.66
Salamonie	0.51	1.37	1.98
Cataract	0.25	0.65	0.94
Brainard	0.00	1.31	1.89
Whitewater	0.25	0.20	0.28
Saluda	0.00	0.85	1.23
Dillsboro	0.63	0.59	0.85
Kope	0.51	0.65	0.94
<i>mean</i>	0.34	0.76	
<i>Mean True Dip</i>			1.10
<i>True Dip Direction</i>			25.4°

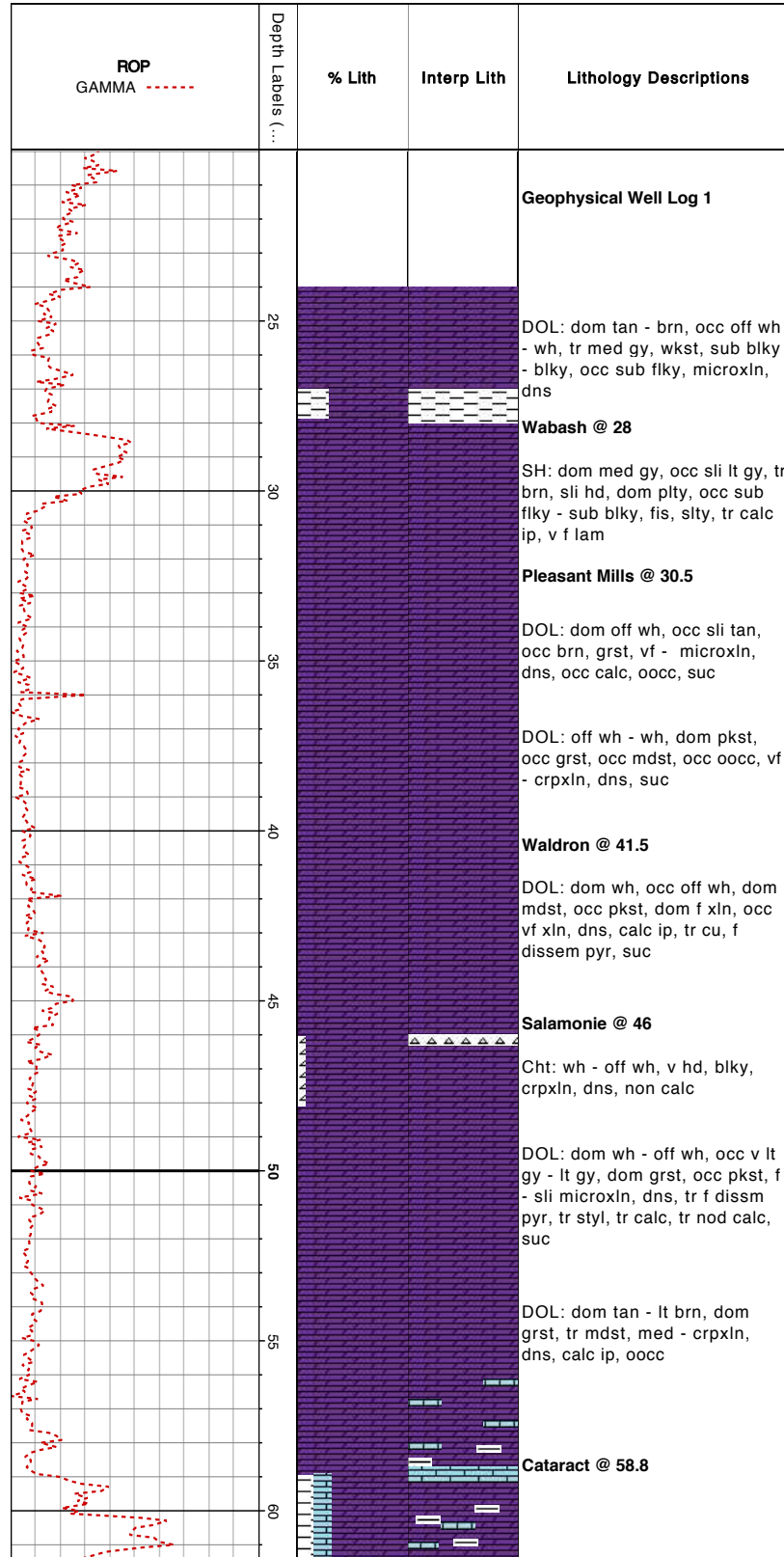
<b>Table 5: Matrix Permeability of Irving Bros. Core</b>		
<b>Depth (M)</b>	<b>Formation</b>	<b>Permeability (M<sup>2</sup>)</b>
3.0	Pleasant Mills	1.49E-15
14.3	Pleasant Mills	9.8700E-17
21.9	Salamonie	3.53E-15
28.3	Salamonie	2.15E-16
32.0	Cataract	1.92E-15
39.0	Cataract	2.19E-14
52.7	Ft Atkinson	7.94E-16
57.9	Whitewater	3.06E-15

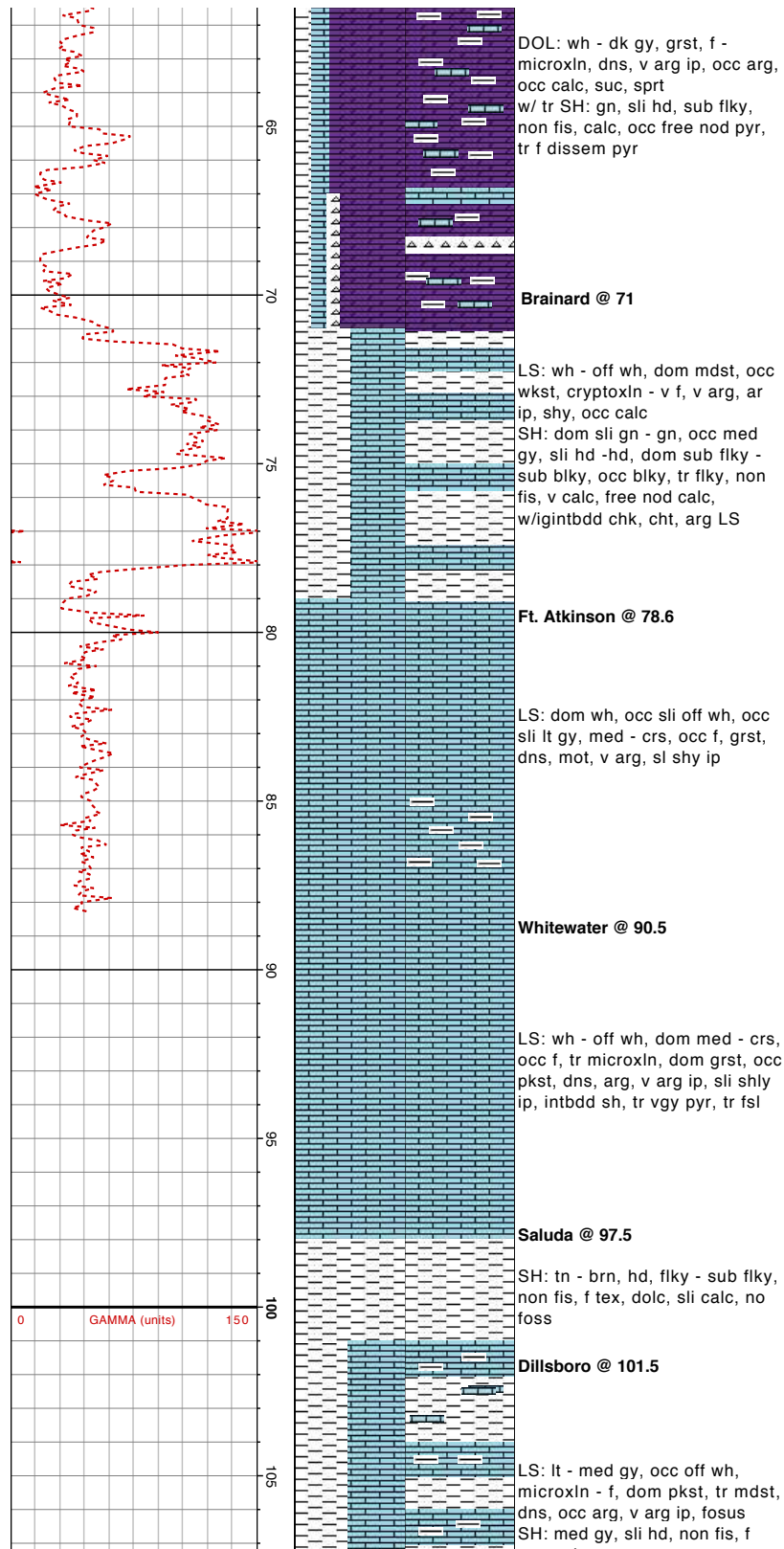
Table 6: Porosity of Irving Bros. Core						
Depth (M)	Formation	Weight Wet (g)	Weight Dry (g)	Water (cc)	Rock Volume (cc)	Porosity (%)
3.0	Pleasant Mills	614.36	598.41	15.95	230	6.9
8.2	Pleasant Mills	395.5	390.27	5.23	80	6.5
10.4	Pleasant Mills	323.8	305.1	18.7	130	14.4
12.2	Waldron	392.95	386.37	6.58	140	4.7
14.3	Waldron	280.58	273.23	7.35	100	7.3
21.6	Salamonie	394.98	372.18	22.8	145	15.7
23.8	Salamonie	914.91	889.57	25.34	345	7.3
28.3	Salamonie	658.02	632.34	25.68	255	10.1
35.4	Cataract	294.95	292.2	2.75	100	2.8
39.0	Cataract	273.73	268.91	4.82	100	4.8
48.8	Brainard	443.16	438.15	5.01	155	3.2
53.0	Ft Atkinson	845.06	831.75	13.31	310	4.3
57.9	Whitewater	644.13	624.55	19.58	230	8.5
62.2	Whitewater	364.41	353.19	11.22	130	8.6

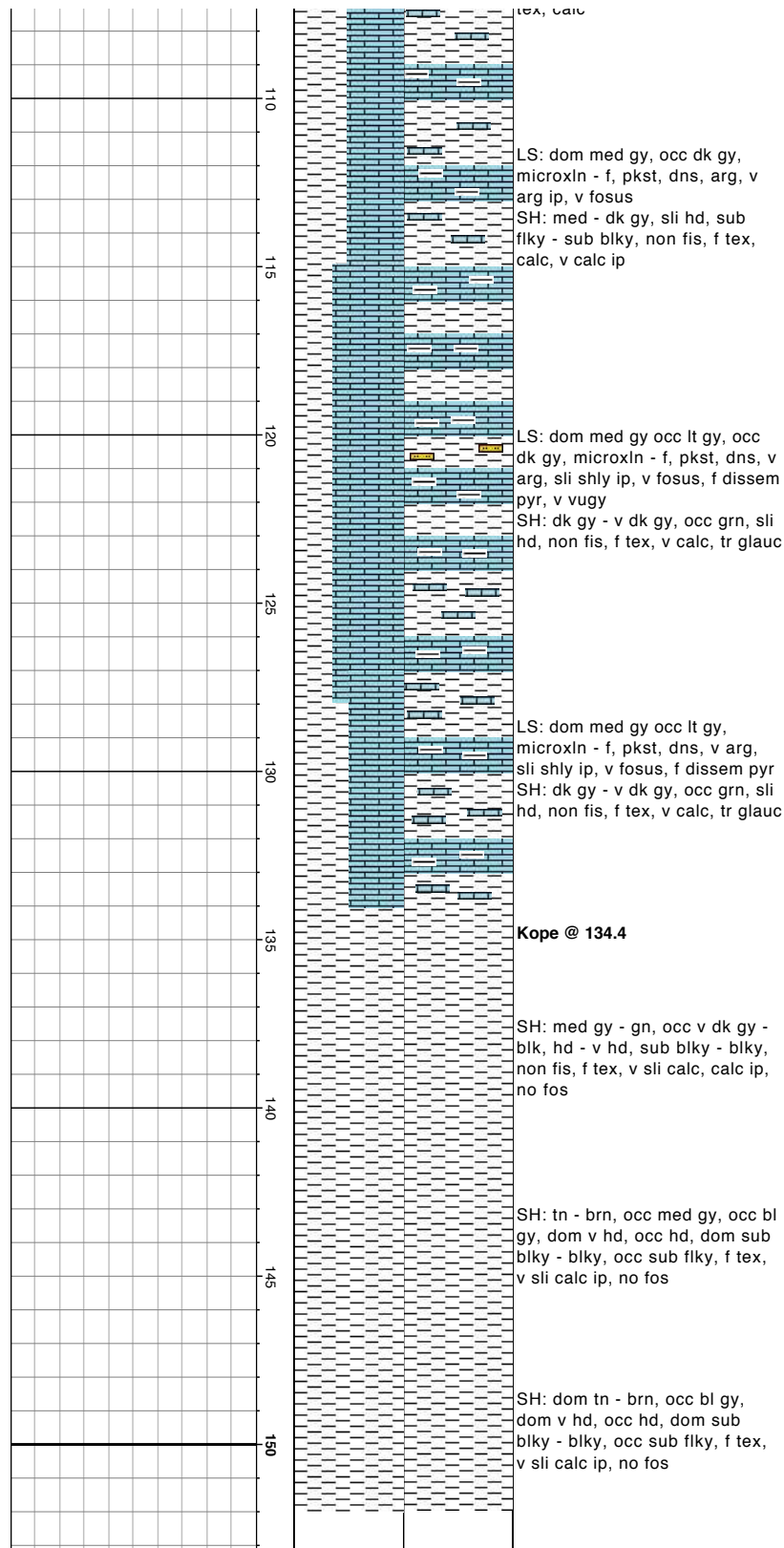


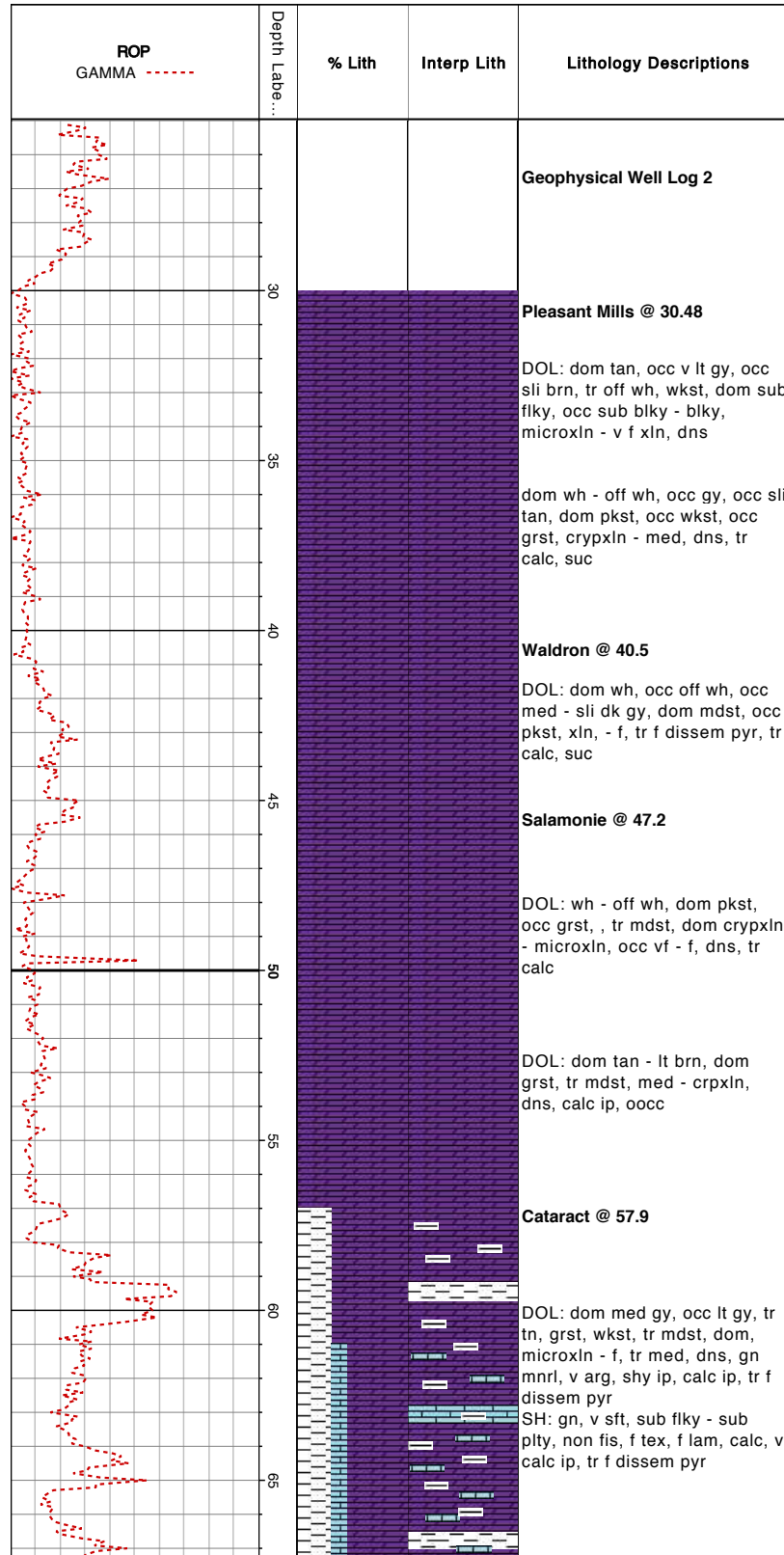
## Appendix 1: Geophysical Well Logs

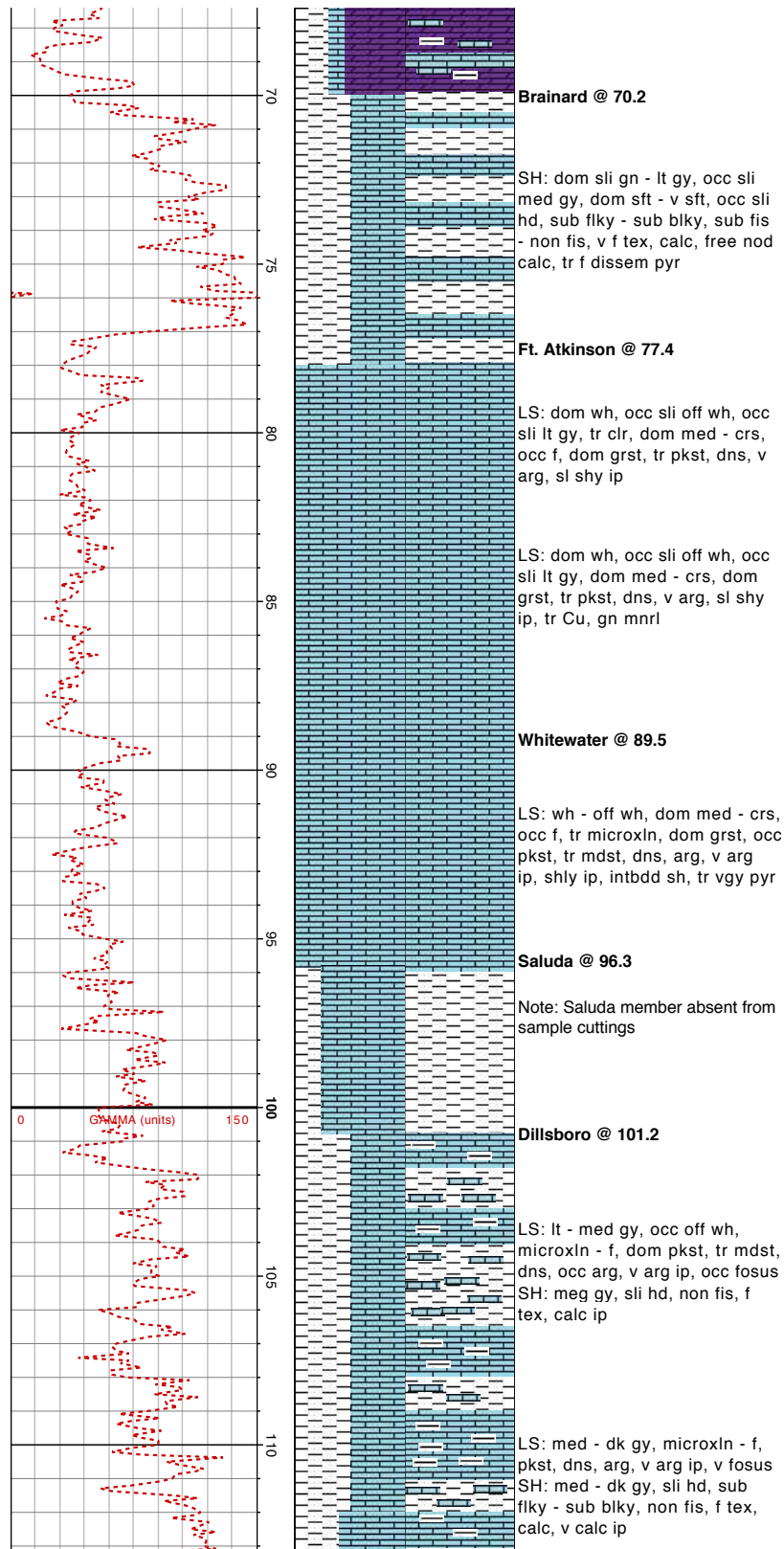






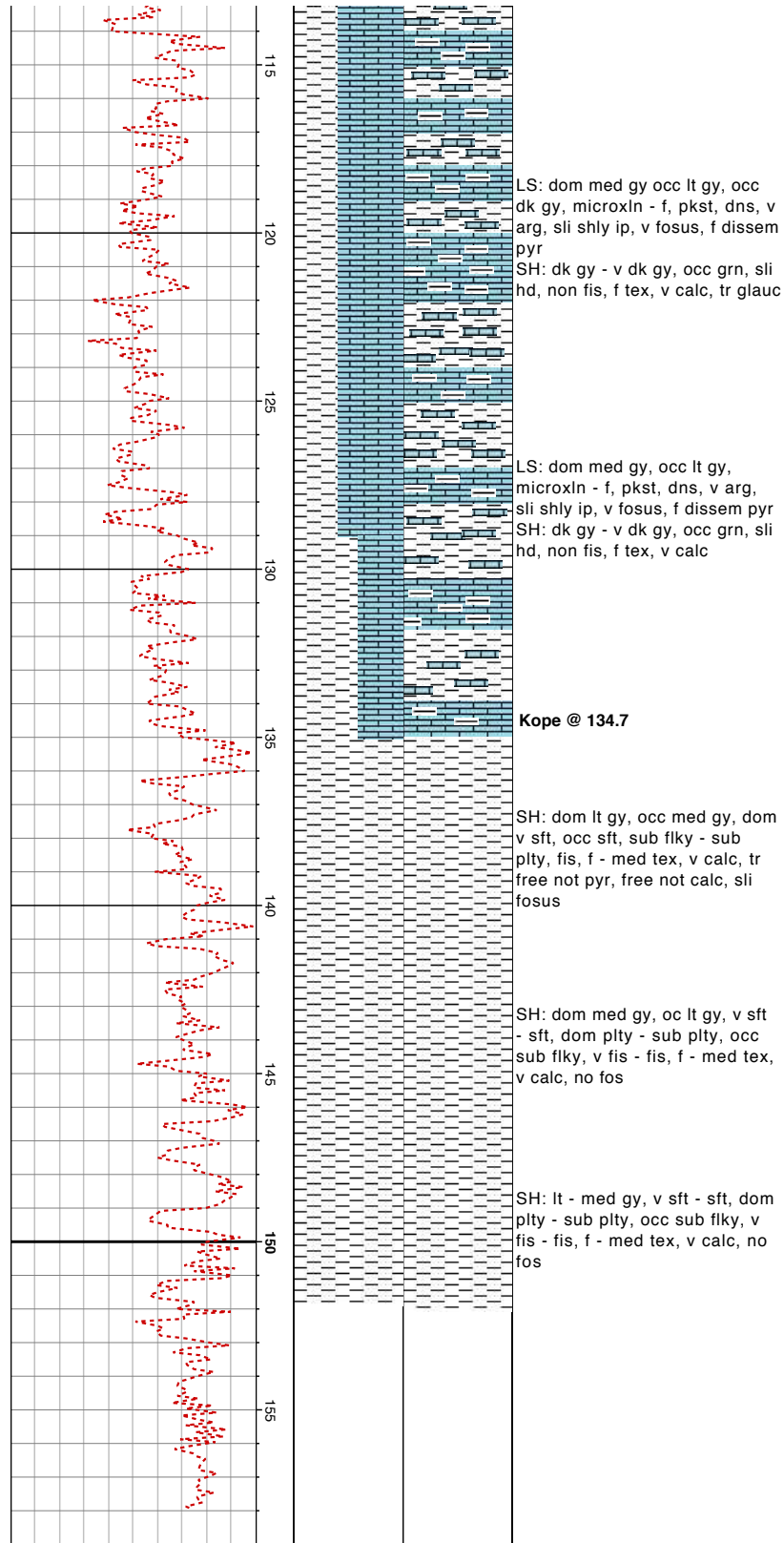




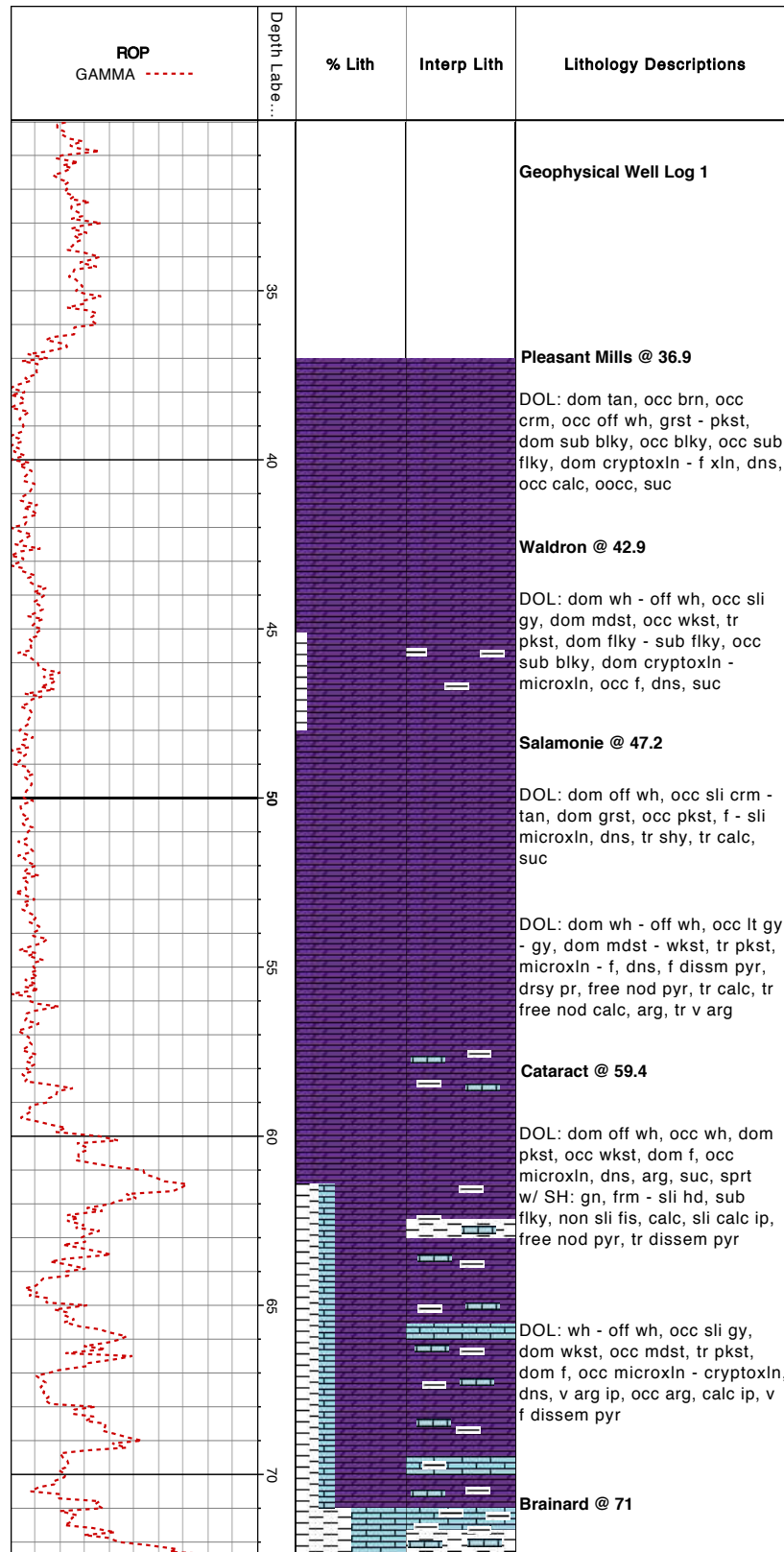


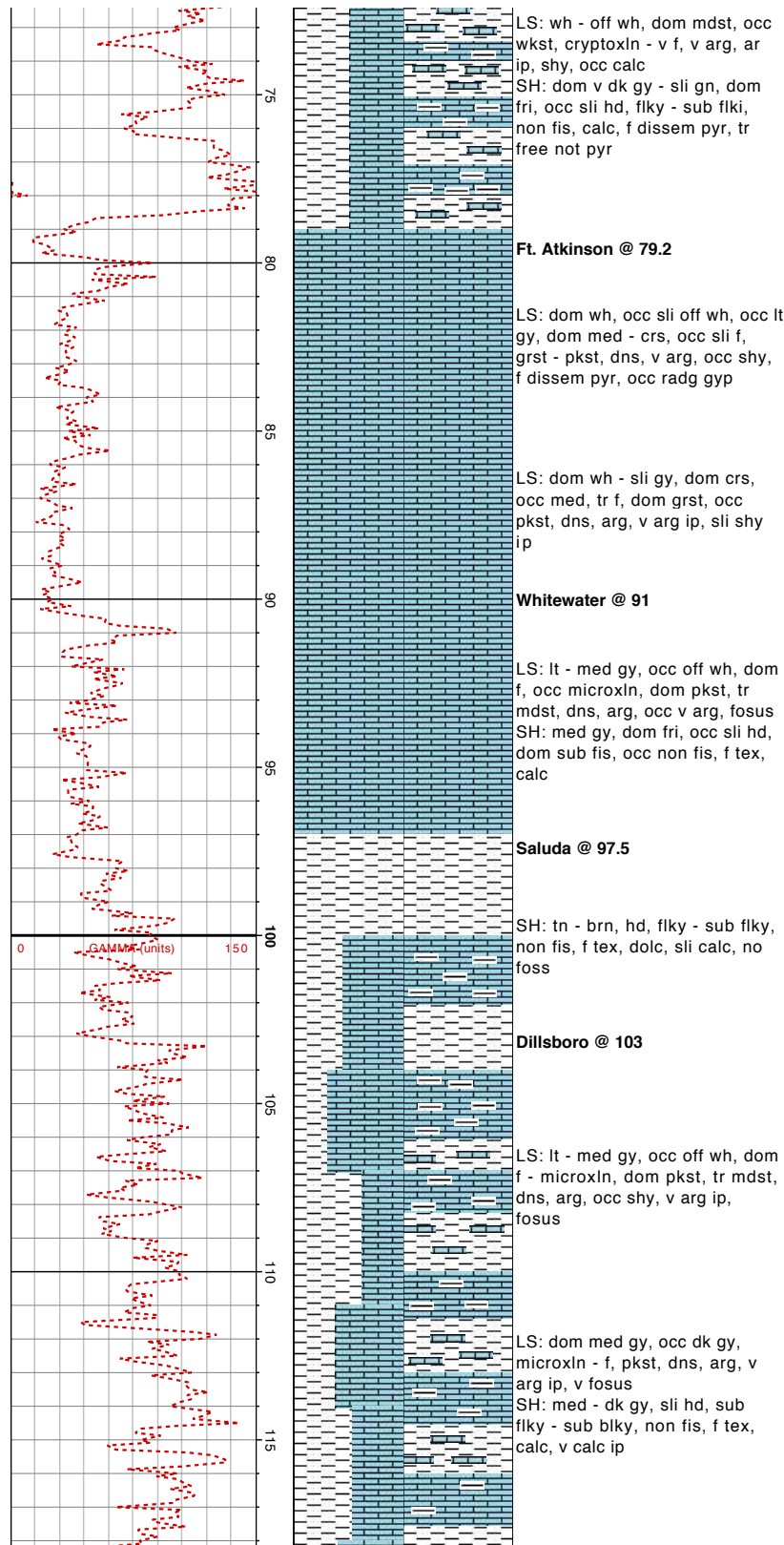


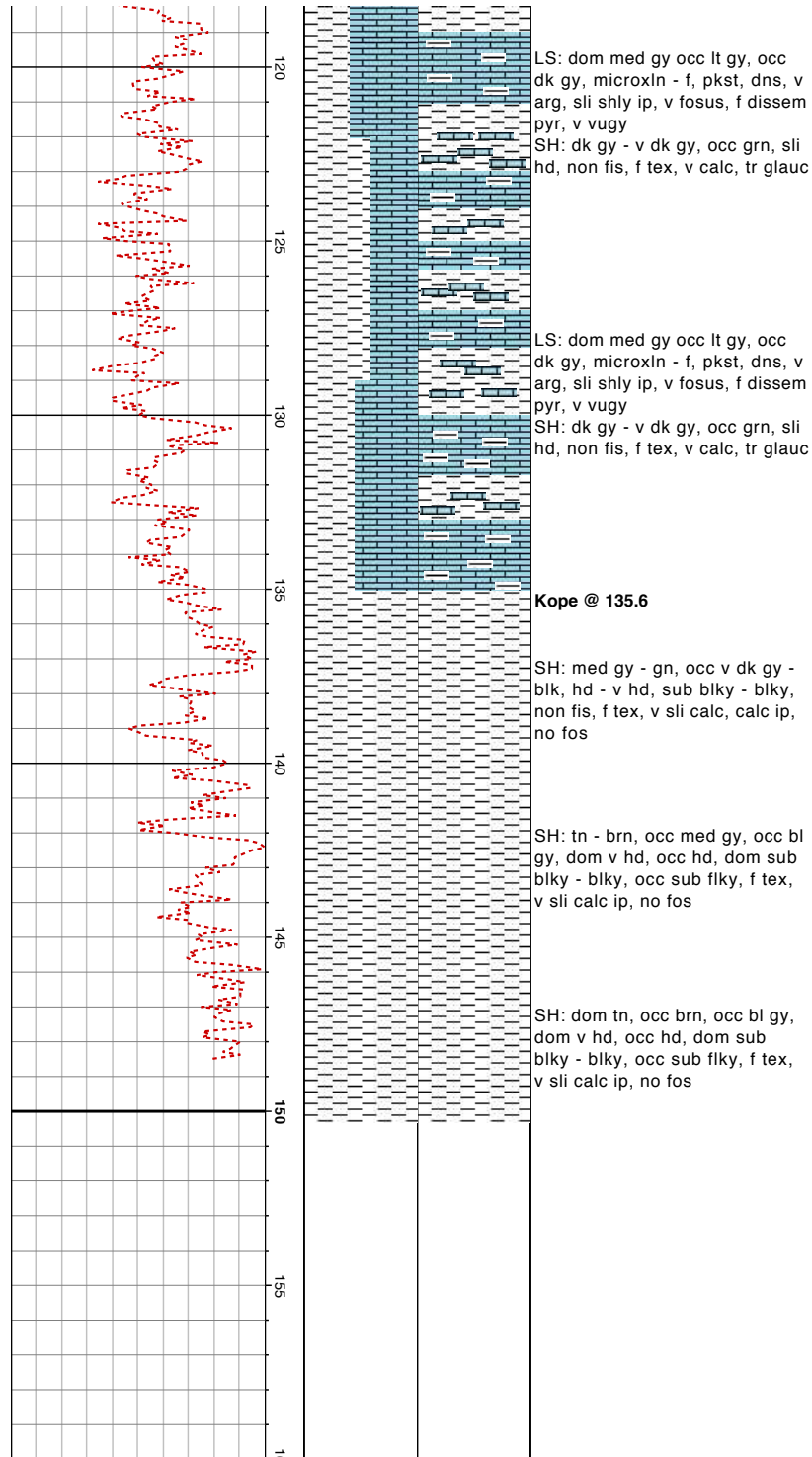


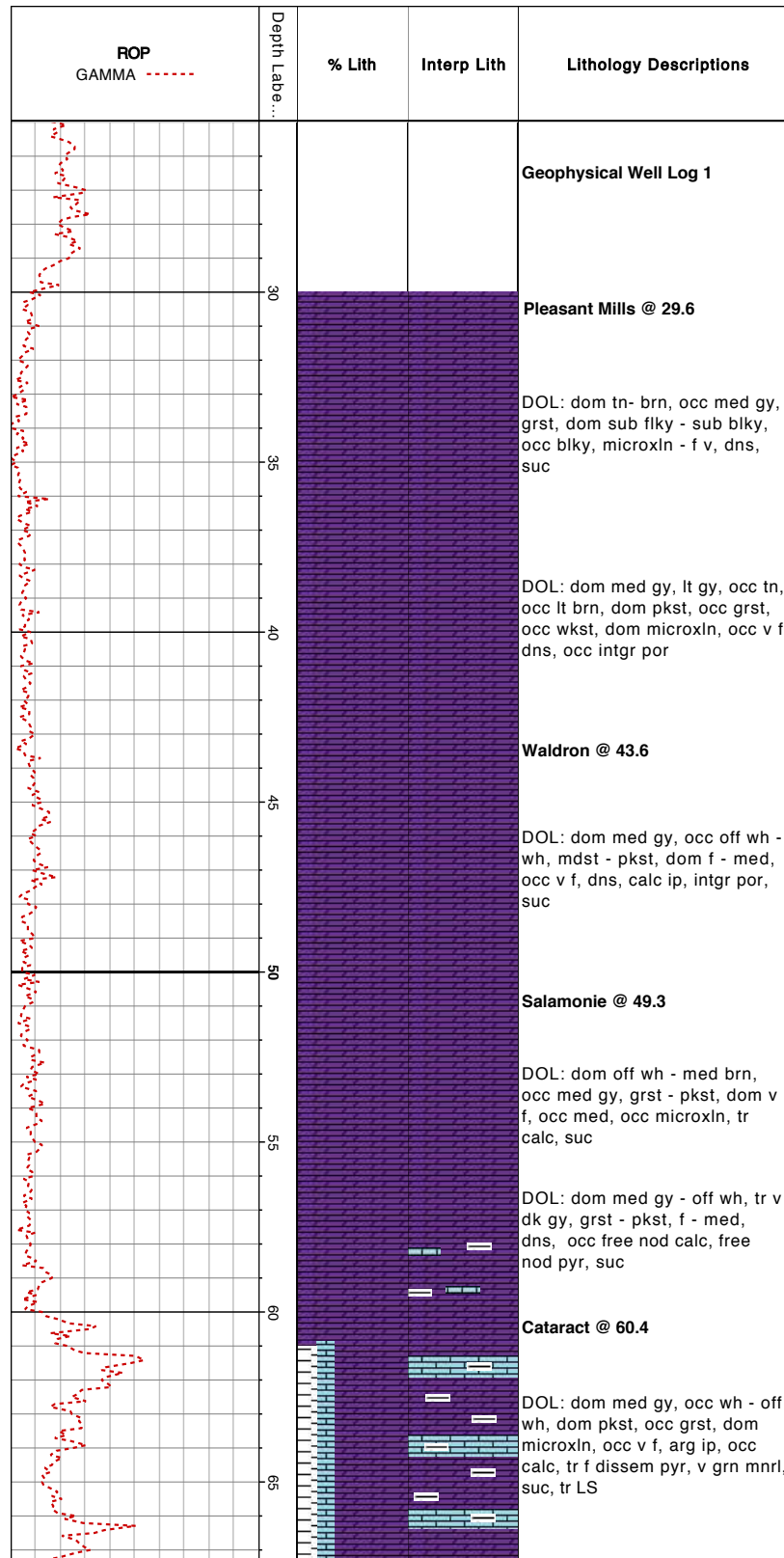


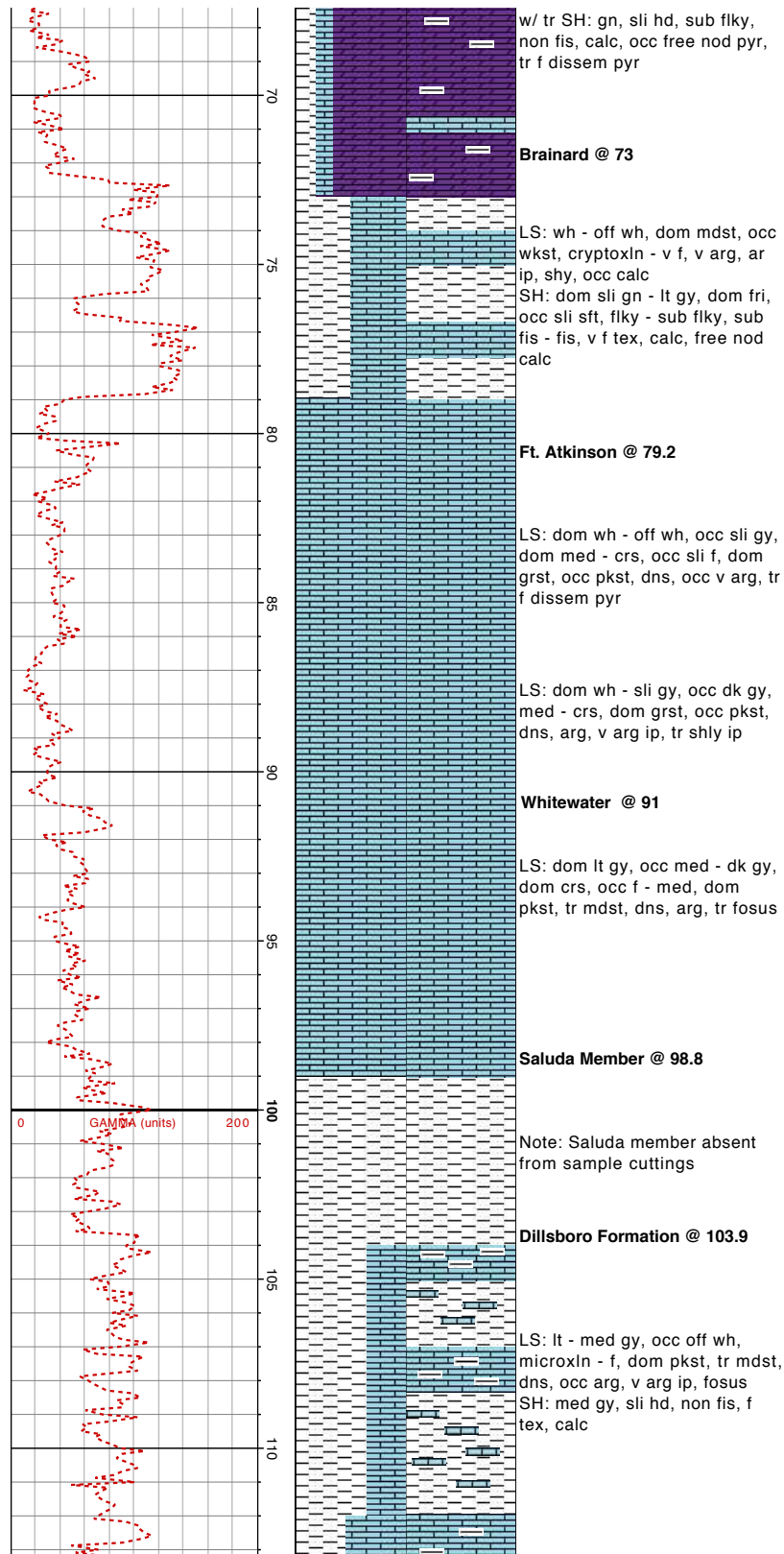




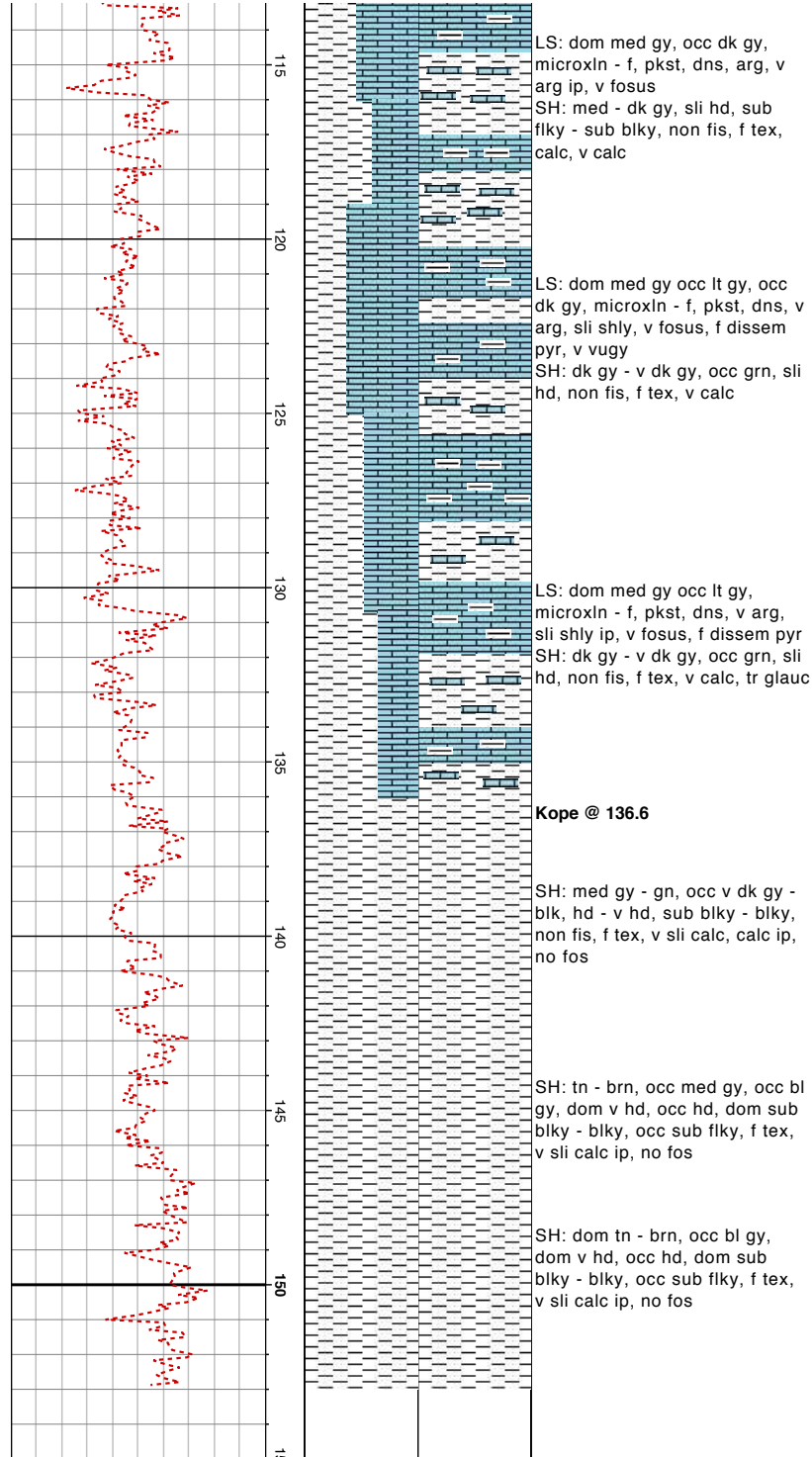












[illegible]



[illegible]







[illegible]







Thin Sec/ Rx Sample	LITHOLOGY	DEPTH (ft)	RECOVERY	PORE TYPE	PHYSICAL/ BIOGENIC STRUCTURES, SURFACES, CONTACTS	FABRIC	Mean Grain Size (TEXTURE)	FOSSIL TYPES	INDURATION	FACIES	COMMENTS
				INTER-PART MOLDIC FRACTURE		Mudstone Wackestone Silty Mault Normal Mud Well Washed Poorly Washed Silstone GS Normal Sand	MUD SILT VERY FINE L. FINE U. FINE MEDIUM L. MEDIUM U. COARSE GRAVEL	Miliolidae Other Forams* Echinoids Bryozoans Red Algae Green Algae Bivalves Gastropods Coral Other*			Siltstone
		151									151
		162								log uc Succin	Wh. texture - 166
		170									
		175								Pyrite	
		181									











[illegible]















[illegible]

WELL NAME:		COUNTY:		INTERVAL DESCRIBED:		PAGE:				
LITHOLOGY	DEPTH (ft)	RECOVERY	PORE TYPE	PHYSICAL/ BIOGENIC STRUCTURES, SURFACES, CONTACTS	FABRIC		FOSSIL TYPES	FACIES	COMMENTS	
					Wackestone	Mudstone				
Thin Sec/ Rx Sample			INTR-PART MOLDIC FRACTURE		Stily Matrix Normal Mud Well Washed Poorly Washed Silstone Normal Sand	MEAN GRAIN SIZE (TEXTURE)	Miliolidae Other Forams* Echinoids Bryozoans Red Algae Green Algae Bivalves Gastropods Coral Other*			
						GRAVEL L. COARSE L. MEDIUM L. FINE VERY FINE SILT MUD				
	180									Blue
	185									interbedded shale / ls gy / wh crossbedding
	190									Brinard @ 184'
	195									no fossils in shale
	200									interbedded shale and limestone every few mm
	205									Siltstone



### Appendix 3: ERT Inversion Models from Mundell et al. (2012)

